Perovskite Solar Cell: Fabrication and Characterization

A Dissertation

Submitted in partial fulfilment of the requirements

for the award of the degree

of

Master of Technology

in

Nanotechnology

By

Dixit Khandelwal

(17551004)

Centre of Nanotechnology

INDIAN INSTITUTE OF TECHNOLOGY ROORKEE

ROORKEE – 247 667 (INDIA)

June, 2019

DECLARATION

I hereby declare that the work presented in dissertation entitled "**Perovskite solar cell: fabrication and characterization**" submitted in partial fulfilment of the requirements for the award of degree of **Master of Technology** in **Nanotechnology, Indian Institute of Technology Roorkee**, is an authentic record of my work carried out under the supervision of Dr. Kaushik Pal, Associate Professor, Department of Mechanical and Industrial Engineering, IIT Roorkee and in collaboration with Dr. Nripan Mathews, Associate Professor at the School of Materials Science and Engineering, Nanyang Technological University, Singapore. The matter embodied in this has not been submitted by me for the award of any other degree.

Dixit Khandelwal

Enrolment No: 17551004

Date:

CERTIFICATE

This is to certify that above statement made by the candidate is correct to the best of our knowledge.

Dr. Kaushik Pal
Supervisor
Associate Professor
Department of Mechanical and Industrial Engineering
Indian Institute of Technology Roorkee

ACKNOWLEDGEMENT

I take this opportunity with my pleasure to thank all the people who have helped me through the course of this journey towards producing this dissertation.

Firstly, I would like to express my profound gratitude and record my sense of obligation to my both the supervisors Dr. Kaushik Pal, Associate professor, Department of Mechanical and Industrial Engineering, Indian Institute of Technology Roorkee and Dr. Nripan Mathews, Associate professor, School of Material Science and Engineering, Nanyang Technological University for their valuable and continued guidance. I am deeply indebted to them for their encouragement throughout, till the completion of my entire dissertation report. It is my privilege that they bestowed me with the opportunity to work in this field.

I owe special thanks to Ms. Bhumika Chaudhary, Ph.D. Scholar, Interdisciplinary Graduate School, Nanyang Technological University for her kind support and guidance as a mentor during the period of my dissertation work at Nanyang Technological University.

Finally, the work would not have been possible without the confidence, blessings and support of my parents, family members and friends. I would like to convey a big thank you to colleagues from Mathews Research Group, Energy Research Institute and Advanced Composite Lab for being pillar of strength and helping me out when in need. Apart from these I would like to also thank to all those who helped me directly or indirectly. I am indebted to each one for their respective contributions.

Date:

Place: **(DIXIT KHANDELWAL)**

CONTENTS

LIST OF FIGURES AND TABLES

LIST OF TABLES

ABSTRACT

Solar cell technology is one of the pivotal divisions of the clean energy sources that have been utilized worldwide for power generation. In that sense, silicon, gallium arsenide, cadmium telluride are conventional materials, in addition with brand-new materials such as perovskites, organic semiconductors and quantum dots. Though, perovskite materials are more fascinating owing to its high efficiency, inexpensive scaling process and greater flexibility which has directed researchers in the field of photovoltaics. However, there are some hassles which hinder the commercialization such as instability due to moisture, elevated temperature and ultra-violate illumination. Many concepts have been reported to improve the stability such as addition of different inorganic cation, mixing of halide anions, changing metal cation, passivation etc. It is because of low ambient stability of the three dimensioanl (3D) perovskites that dictates the research to new path of mixed dimensional 2D/3D perovskite. This approach is adopted as an alternative way to stabilize perovskite. A ligand with large organic cation is hydrophobic in nature which in turn are used for the formation of hybrid 2D/3D perovskite. In this report, preliminary study is done on an organic pseudohalide based ligand which is used as an additive to enhance the ambient stability of perovskite solar cells in day-to-day life.

Key words: Perovskite solar cell, Hybrid 2D/3D perovskite, Stability

CHAPTER 1: Introduction

1.1: Energy sector scenario

Conventional methods of energy generation require fossil fuel, which is not that much abundant source. Renewable energy sources are the only abundant source of energy which can help to overcome from this tremendous need of energy in longer run. Renewable energy sources are also called as clean energy sources because they are pollution-free and helps to reduce the green house effects.

In 2005, renewable energy of total electricity generation was merely 2% which increases to 6.3% in year 2014. According to world energy outlook 2017 report of International Energy Agency (IEA), the world-wide energy demand will increase to 30% by 2040 of which 40% of this demand will be met by clean energy technologies [5].

The traditional approach of generating clean energy were solar energy, wind energy, biomass, tidal, and geothermal energy. Among these, the solar energy harnesses the most due to earth receiving 2.9×10^{15} kW energy per day from the sun, which is hundred times in magnitude than what is our consumption in a year. Therefore, the solar energy is gaining the higher attention and developing with fast pace.

1.2: History of photovoltaics

In the early 1900s semiconductor materials were discovered with some weird electrical properties. Semiconductor shows negative temperature coefficient of resistance and intermediate properties than metal and insulator. In energy sector applications, it has shown huge potential like light absorbing material as a solar cell and light emitting material as LED.

First photovoltaic effect was experimentally demonstrated by physicist Edmond Becquerel in 1839. Later, huge research work on solar cell gained prominence with their incorporation on Vanguard I satellite in 1958. It was used in satellite as an alternative power source due to which application of solar cell arrays in the satellite become a common feature. Solar cell gained more market because it showed high power to weight ratio. For the space application, power source cost could be high. Therefore, initially cost was not the problem for solar cells which led research in the direction of higher efficiency. In early 1990s GaAs was found as a better substitute to silicon

solar cells. To expand the application domain of the solar cell in terrestrial application has changed the direction of research and came up with new promising materials with less cost.

1.2.1: Development of solar cell technology:

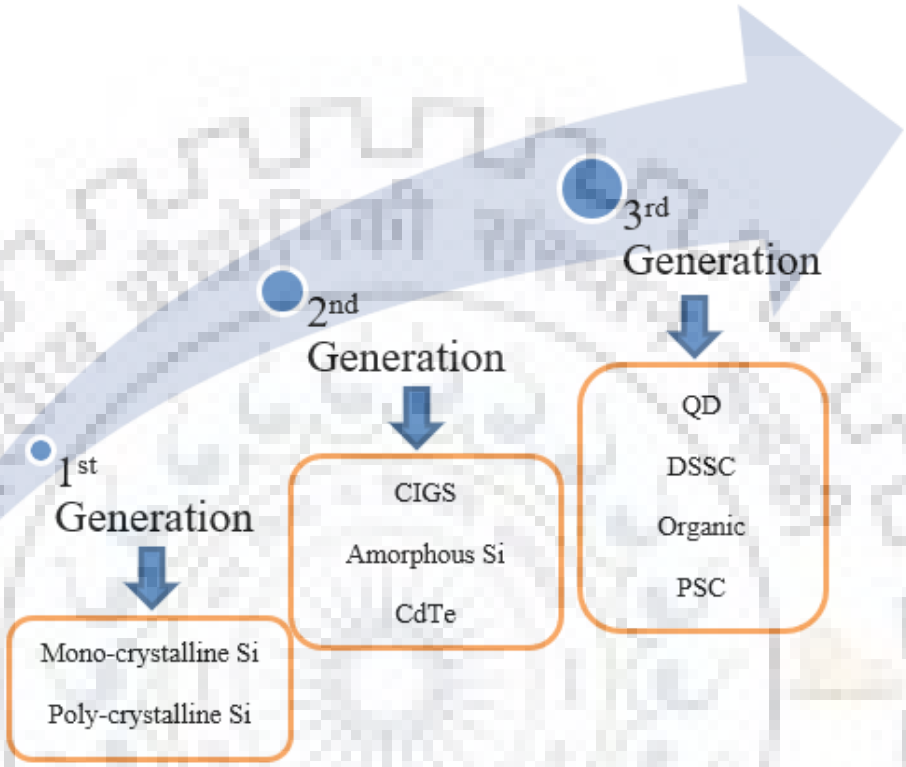

Figure 1.1: Development of solar cell technology

- **1st Generation: wafer based**

In the early era of solar cell development crystalline silicon wafer was widely used. This generation also called as the wafer based crystalline silicon solar cell. Crystalline silicon is categorised in monocrystalline and polycrystalline silicon. In monocrystalline silicon, the lattice parameter, its orientation and electronic properties are remains constant which helps in good power conversion efficiency. While plenty of small crystals are present in the polycrystalline Si, so that the cost of the cells can be reduced as compared to monocrystalline but with compromising the efficiency.

It has large area and single p-n junction. It reached up to maximum efficiency of nearly 25%, while single junction cells has nearly 31% efficiency as Shockley Queisser limit. The advantages of these solar cells were broad spectral absorption range and higher carrier mobility (at 300K, 1400 cm^2 /

(V·s)) [6]. These cells are expensive to manufacture, most of the photon energy gets wasted and decrease in the efficiency when temperature increases.

- **2nd Generation: Thin film based**

These generation solar cells were manufactured based on thin film technology and with other new materials like amorphous silicon, Cadmium Telluride (CdTe) and Copper Indium Gallium Di-selenide (CIGS). The aim was to overcome the limitation of the first generation cells i.e. comparative low cost and reduced mass. So the active material used has very less thickness with higher light absorption capacity.

For CdTe, maximum efficiency achieved is nearly 22% and the theoretical efficiency of these cells are too high than the other semiconductors. CIS has advantage of its light weight and flexibility.

The problem with this generation solar cells was toxicity of Cd material and it limits the mass production because of the scarce material Tellurium.

- **3rd Generation: emerging thin film based**

These generation cells are developed to get the advantages of previous both the generation cells. This modern technology has created Dye-synthesized solar cell (DSSC), organic solar cells, and QD (quantum dot based) solar cells etc. which are having the more efficiency, durability and simple processing. Still the development is going on the usage of more abundant and non-toxic materials.

Quantum dot solar cells has size dependent tunable bandgap. It has low efficiency still it got attention because of its versatile properties like light weight and low cost.

Organic solar cell uses organic molecule to absorb light and to transport charge carrier. Processing is cheap for these materials but the problem with its stability, low efficiency.

DSSC works on the principle of photo-electro-chemical process. It consists of TiO_2 nanoparticles, Dye-particles and electrolyte. Where the role of the dye-sensitizer is to donate electron, TiO_2 nanoparticles accepts electron and electrolyte is ionized solution of iodine to conduct electricity. Which stands as a promising technology for solar cell but the problem was its stability of electrolyte under various weather conditions.

Perovskite mineral was used in solar cell for the first time in 2009 by Miyasaka, where they coated thin layer of perovskite on TiO_2 particles then used in DSSC. The power conversion efficiency (PCE) of perovskite solar cells has quickly increased from 3.8% to 23.7% (NREL certified) [7] in less than a decade. It gaining the attention not only due to higher efficiency but also due to cheaper manufacturing.

Here, the rapid progress of perovskite solar cells certified efficiency has shown in graphical format in the figure below.

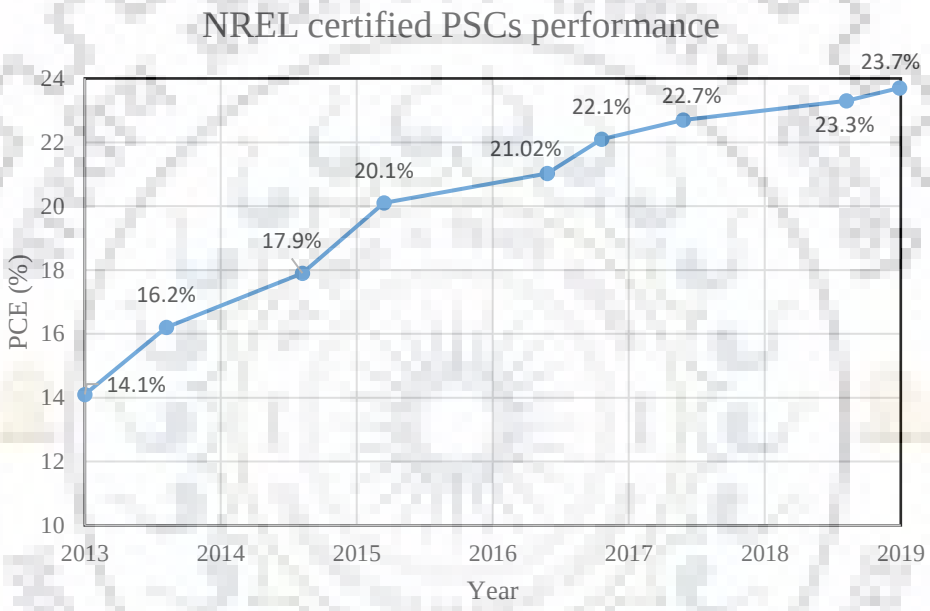

Figure 1.2: Efficiency growth for perovskite solar cells

CHAPTER 2: Literature review: Perovskite solar cell

2.1: Introduction to perovskite

Gustav Rose discovered the mineral $CaTiO_3$ (Calcium Titanate) in 1839. Russian Mineralogist L. A. Perovski, who did research on those minerals and shown that these minerals are showing different crystal structure than conventional ones, so that crystal structure named as Perovskite [8].

The general chemical formula for these materials is ABX_3. Where A is big-cation located at the corners while B is small-cation located at the body centre and X is anion located at the centre of all the faces.

Figure 2.1: Perovskite crystal structure

For perfect cubic perovskite structure it has to follow the relation(eq.(i) &(ii)) with t = 1[9].

$$t = \frac{R_A + R_X}{\sqrt{2} * (R_B + R_X)} \ldots\ldots\ldots (i)$$

$$\mu = \frac{R_B}{R_X} \ldots\ldots\ldots (ii)$$

Where,

t = Tolerance factor, μ = Octahedral factor, R_A = Radius of A site cation,

R_B = Radius of B site cation, R_X = Radius of X site anion.

Tolerance factor was given by Goldschmidt in 1926 as an indicator of the crystal stability and distortion of the crystal structure, so it can be used to check the compatibility an ion in the crystal structure [9]. If tolerance factor has value greater than 1 then it will show hexagonal or tetragonal structure, cubic structure for $0.9 < t < 1$, orthorhombic/rhombohedral structure for $0.71 < t < 0.9$ by tilting the octahedral geometry to fill the space, while for values less than 0.71 it can show different structure. For A cation to fit into the cavity it must have to satisfy tolerance factor criteria with $t \leq 1$ [10]. Octahedral factor shows the octahedral co-ordination of the B metal cation by six X anion.

Four unique mechanism that are related to deformation of perovskite structure which can induce wide range of properties in perovskite:

- The tilting of the octahedral cage
- Off-centering of the octahedrally coordinated cations
- Distortion of the octahedral cage
- Off-centering of the 12-fold coordinated site

These deformations induces various properties like shown in table below. Due to this much variety of properties it can be used in the field of mulita-layer ceramic capacitor, storage and switchable devices, solar cell, Light emitting diode etc.

Table 2.1: Various properties of different perovskites

Di-electricity	Ferro-electricity
Piezo-electricity	Pyro-electricity
Semiconducting	Super conducting
Charge ordering	Linear/non-linear optics
Spin dependent transport	Catalytic conversion

2.2: Properties of lead-halide perovskites

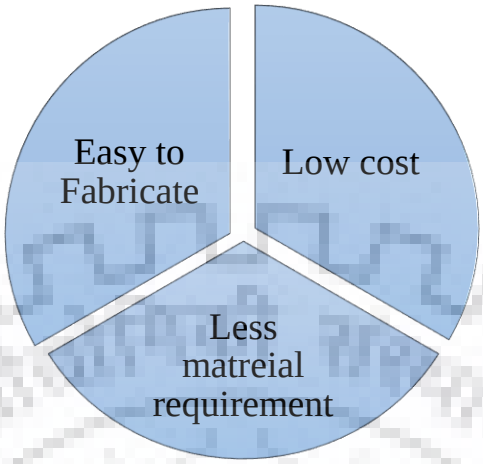

Figure 2.2: Advantages of lead-halide perovskites

Lead halide based perovskites can be generalize as $APbX_3$ where, A is cation, and X is halide anion. These Perovskites are exhibiting high absorption in visible region of solar spectrum due to which its thin film can absorb maximum photons and able to generate charge carriers, so less material is require for the solar cell application. It can be modified to achieve bandgap from 1.3 eV to 2.3 eV that can be tuned to have better spectral utilization of solar spectrum. It possess relatively longer recombination lifetime, and higher carrier mobility which helps in field independent exciton dissociation. Apart from these properties it is defect tolerant material so that it can be spin coated easily to fabricate solar cells without losing its performance. Costing of processing perovskite is very less as they are spincoated to prepared thin films.

2.3: ABX_3 composition-size-structure-optical property interrelation

The metal cation and halide anion plays major role in electronic band structure, while A site doesn't participate straight to the electronic band structure but it affects the hybridization that takes place between metal cation and the halide anion due to their orbital overlapping. For $MAPbI_3$ perovskite, lead and iodine octahedral cage has sp^3d^2 hybridization where 5p orbital of iodine forms upper valance band and lower conduction band formed by 6s-6p orbitals of lead.

The nature of bond between the organic cation and the inorganic cage is purely ionic. There is charge induced dipole in the organic molecule so charge-dipole interaction appears between organic dipole and the inorganic network which is dependent on the molecular orientation. The

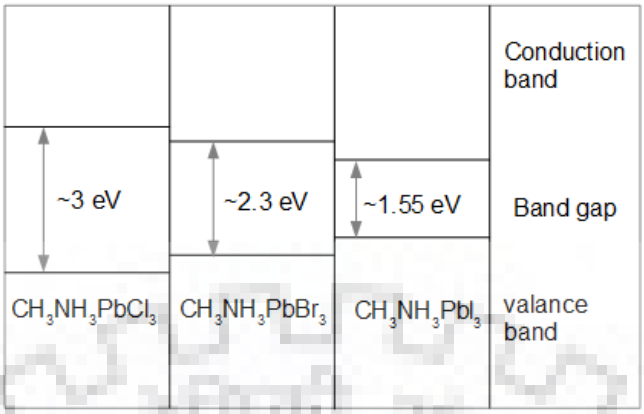

Figure 2.3: Effect of halide anion on bandgap of perovskite

polarization of the lattice provides an additional advantage to the perovskite that the internal electric field helps in the charge separation, improved carrier lifetime, and V_{oc} above the bandgap of the material, which makes it suitable for solar cell application.

2.3.1: Effect of A site cation:

In ABX_3, substitution of the A cation will alter the crystal geometry. If the cation size is reduced then the bandgap will increase as seen from table below for $APbI_3$ [11]:

Table 2.2: Size effect of A site cation on bandgap

A site	**Bandgap**
$CH_3NH_3^+$	1.55 eV
NH_4^+	0.3 eV
H^+	<0.3 eV

The A site cation is playing two major role:

1. Neutralises the charge of the octahedron network
2. Filling of the cubic void generated between octahedral network

The A site can be filled by inorganic or organic cation which divides in two major class of perovskite i.e. organic-inorganic hybrid perovskite and inorganic perovskite. As the A site has to fill the void created between the octahedral network, which has limited space so it can

accommodate only small sized cation with three or less C-N/C-C bonds to make a three dimensional structure.

If the size of A cation is large enough compared to B metal cation then it will slicing off the three dimensional perovskite into lower dimensional perovskite called 2D or quasi-2D or may be in 1D.

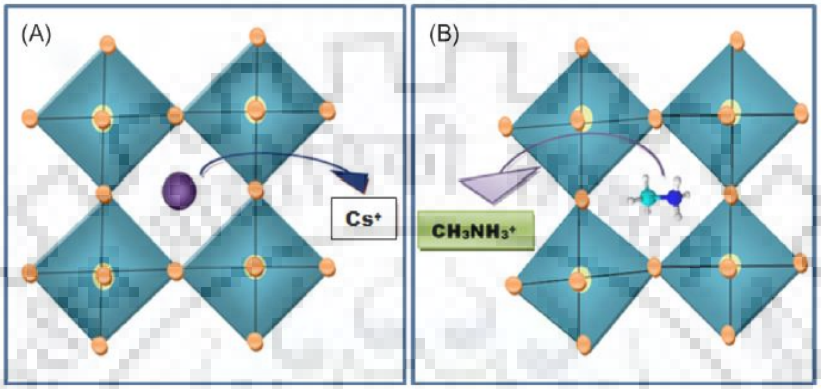

Figure 2.4: (a) Inoganic perovskite, and (b) Organic perovskite

2.3.2: Effect of B site cation:

Metal cation will directly change the conduction band as talked earlier because of its s and p orbital. If the size of the metal cation is reduced then it shows increase in the bandgap. Table below shows as size of cation increases bandgap decreases for $MABI_3$.

Table 2.3: Metal cation effect on bandgap

B site	Bandgap
Pb	1.55 eV
Sn	1.7 eV
Ge	2 eV

2.3.3: Effect of X halide anion:

The halide anions are more effective candidate for changing the bandgap, substitution of them will leads to more shift in bandgap compared to organic cation. As the halide anion size decreases the bandgap increases because the halide anion outer orbital compose the valance band. Cl, Br, I has outer orbital 3p, 4p, 5p respectively will give reduction in the bandgap. So, electron binding energy

will decrease as moved from Cl to I. mixing of I and Br halide tend to improve the thermal stability because of their comparable ionic sizes. Table shown is for $MAPbX_3$.

Table 2.4: Effect of halide ion on bandgap

X site	Bandgap
Cl	3 eV
Br	2.3 eV
I	1.55 eV

So this technology promises for:

Low cost	Thin layer (less material)
High efficiency	Light weight solar cell
Flexible solar cell	Terawatt scalability

2.4: Perovskite as a solar cell

In 2009, Kojima et al. [3] demonstrated the use of organic lead halide perovskite as visible light sensitizer self-assembled on TiO_2 in liquid-electrolyte based DSSC. $CH_3NH_3PbI_3$ and $CH_3NH_3PbBr_3$ perovskite were used as a light sensitizer. $CH_3NH_3PbI_3$ based cell exhibited

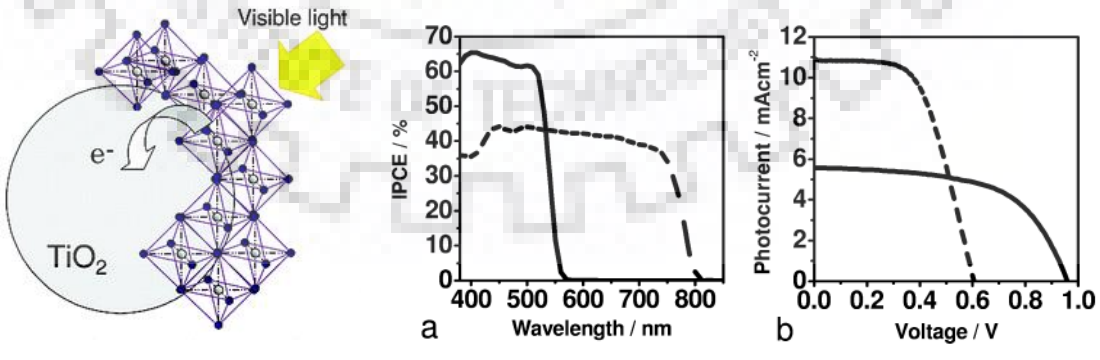

Figure 2.5: (a) IPCE spectra for $MAPbI_3$ and $MAPbBr_3$ cells (b) I-V characteristics for cells (c) Perovskite nano-crystalline sensitizers on TiO_2 [3]

efficiency of 3.81%, while $CH_3NH_3PbBr_3$ exhibited efficiency of 3.13% when measured on effective incident area of 0.24 cm^2 under 100 mW/cm^2 with AM1.5 simulated sunlight irradiation. They also reported that the value of V_{oc} (open circuit voltage) for $CH_3NH_3PbBr_3$ (0.96V) is higher than the $CH_3NH_3PbI_3$ (0.61V).

Nam-Gyu Park and co-worker [1] fabricated 2-3 nm sized quantum dots of $CH_3NH_3PbI_3$ on TiO_2 surface, using this with the iodide/iodine based redox electrolyte they achieved solar to electrical conversion efficiency of 6.54% at one sun illumination and AM1.5. They also compared the perovskite quantum dots with the conventional N719 dye as shown in **figure (2.6)** where perovskite QD showed better results than N719 dye which exhibited the 3.89%.

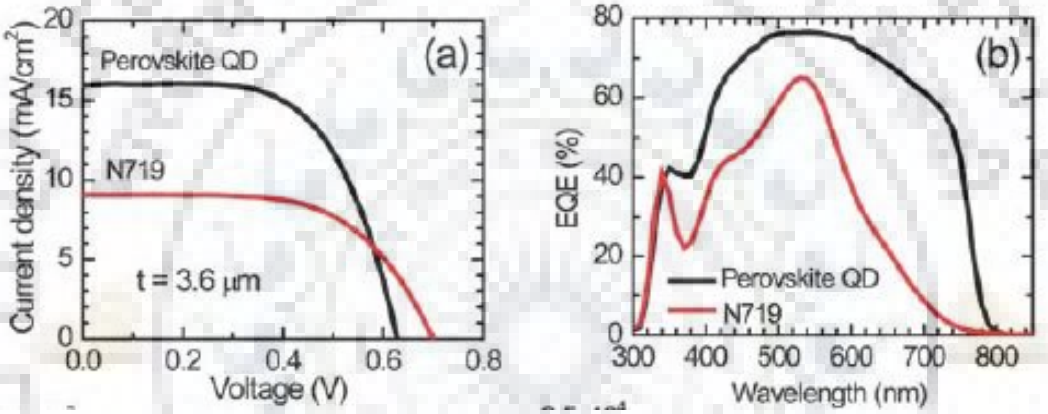

Figure 2.6: Comparison of perovskite QD and N719 dye, (a) I-V and (b) EQE [1]

In 2012, Nam-Gyu Park et al. [4] reported solid-state mesoscopic hetero junction solar cell of $CH_3NH_3PbI_3$ nanoparticles as a light harvester. They used Spiro-OMeTAD [(2, 2, 7, 7 -tetrakis-(N,N-di-p-methoxyphenyl-amine)-9,9-spirobifluorene)] as a hole transporting material and TiO_2

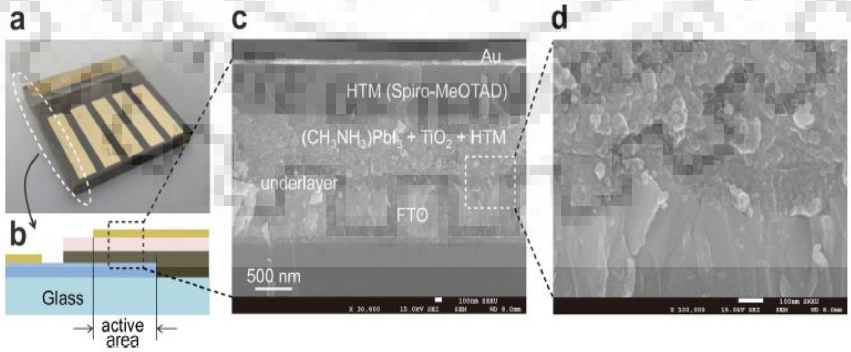

Figure 2.7: (a) Solid state device (b) Crossection of solid-state device (c) Crossectional SEM of device (d) From bottom FTO-underlayer-Active layer [4]

as a mesoscopic scaffold. They reported the efficiency of 9.7% with photocurrent exceeding 17 mA/cm^2. Their approach was highly appreciable because of solid hole conductor material which helps in stability improvement than the liquid electrolyte. The device structure is shown in the **figure (2.7)**.

Henry J. snaith et al. [12] demonstrated a new structured organometallic halide perovskite based hybrid cells with efficiency of 10.9%. They proposed that, it is possible to generate open-circuit voltage more than 1.1V with absorber bandgap 1.55 eV with their method. They claimed that highly crystalline perovskite absorber reduces the losses that are related to the tightly bound excitons and low-mobility. Apart from that they also proved that highly crystalline perovskite absorber has the absorptivity in visible to near-infrared which leads to improvement in efficiency. In their study they included TiO_2 and Al_2O_3 as a mesoscopic scaffold. Although, insulating Al_2O_3 is not participating in the charge transport mechanism it showed better performance, which led to research in new directions. Further in 2013, Henry J. snaith et al. [13] reported low temperature processed perovskite absorber $CH_3NH_3PbI_{3-x}Cl_x$ based thin film perovskite solar cell which achieved power conversion efficiency of 12.3%. Initially the perovskite dye used to be deposited in single step with mesoporous metal oxide but Michael Gratzel et al. [14] proposed a new approach of sequential deposition as a rout to improve the efficiency of perovskite solar cell due to improvement in the morphology of the films. Single step deposition of the perovskite drives to uncontrolled precipitation of the perovskite which leads to large morphological variation. They prepare mesoporous TiO_2 on 30 nm compact TiO_2 under-layer followed by deposition of the PbI_2 layer and then dipping the films in to solution of CH_3NH_3I.

This competition of achieving the higher efficiency resulted in the device engineering, deposition techniques and solvent engineering methods and their advancement bring about improvement in the performance of the solar cells to 22.1% in 2017 and 23.7% in 2018.

2.5: Fabrication and working principle of perovskite solar cell

2.5.1: Deposition methods

For silicon cells processing is multi-step and it is required to process at higher temperature (>1000^{o}C) and under high vacuum condition which incurs high cost of fabrication. So in

comparison with traditional silicon cells, perovskite solar cells required simple processing. It can be solution processed due to its good solubility in common solvents which makes it very robust for solar cells fabrication and cheaper than others [15].

Deposition method had played very important role in development of the high efficiency and stable PSCs. Some parameters like stoichiometry, crystallographic phase and grain structure of perovskite needed to control for better performance of PSCs .

There are mainly four methods for deposition of perovskite light active layer as follows:

1. **One-step process**

This deposition method widely used because of its ease in process and low cost. It can achieve films with suitable density, phase-pure, pin-hole free and with appropriate stoichiometric ratio of perovskite precursor with annealing post-processing.

In this approach, two perovskite precursors are mixed with solvent or mixed solvent and then spin coated followed by annealing in the range of 100-150 ^{o}C.

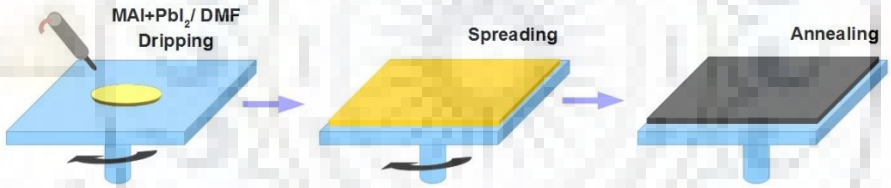

Figure 2.8: One-step deposition

2. **Two-step process**

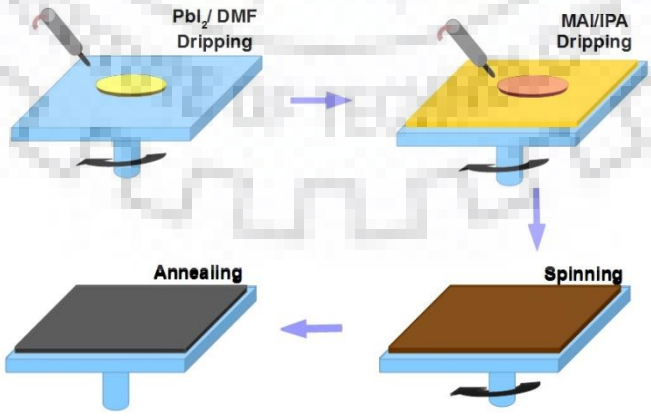

Figure 2.9: Two-step deposiotion

It doesn't require complete preparation of precursors but precursors are coated one by one on substrate. First PbX_2 is deposited followed by the MAX incorporation either by dipping or spin-coating and backing. So diffusion of MAX into PbX_2 lattice takes place.

Adjusting the parameters in either steps can result in the good quality perovskite film and proper morphology.

Sometimes the diffusion process becomes slow due to low temperature and less time of mixing, which brings on the poor cystals of perovskite. However, the negative effect has been noticed on device efficiency for the non-stoichiometry ratio.

3. Thermal-evaporation process

It mostly used for thin film device fabrication. It controls the film composition and surface uniformity are current/voltage and time. The sources are evaporated electrically and gets deposited. For this method low vacuum is required which may little in increase in cost, but thermal-evaporation has advantages like pinhole free and fully covered film.

Figure 2.10: Thermal evaporation

The sources of PbX_2 and MAI are co-evaporated and deposited on rotating substrate as shown in the **figure (2.10)**.

4. Vapor-assisted process

It can be considered as the modified two-step method. This fabrication has to be done in glove box. Ideally, this approach gives healthier connection between precursors than in the solution

process. This technique also evades the incomplete perovskite dissolving which gives improved perovskite film stoichiometry. Annealing will improve stability and power conversion efficiency. The only disadvantage of this method is that it takes hours to complete the process than compared to spin coating which takes minutes to complete process.

Here, first PbX_2 is spin coated on the substrate then the vaporized MAI reacted with prepared film followed by annealing.

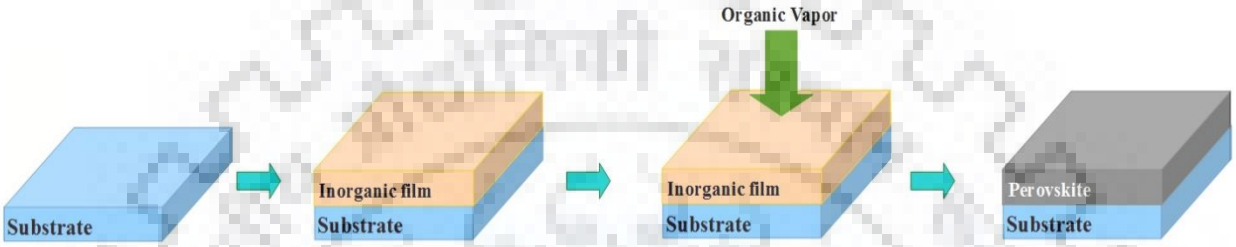

Figure 2.11: Vapor-assisted process for deposition

2.5.2: Device structures

When kojima et. al. [3] made DSSC with perovskite, it was showing the poor stability because of liquid electrolyte used as charge transporting media. Later, when the effort of replacing the liquid electrolyte with solid HTM got success with PCE ~10% with perovskite as an absorbing layer. That was the revolutionary research which opened the new era of various device architectures discussed as follows:

1. **Liquid electrolyte DSSC Structure**

It is the conventional DSSC structure. It comprised of TCO/c-TiO_2/mp-TiO_2 with sensitizer molecular dyes in liquid electrolyte/counter electrode [16] as shown in **figure (2.12)**.

Incident photon will excite the dye molecule and excited electron will move to front anode electrode via conduction band of mesoporous TiO_2. The oxidized dye molecule will return to the ground state by accepting the electron from I^- ion. Diffussion of I_3^- to back electrode will takes place of after donating an electron and regeneration happens by the cathode delivered electron. Here, the V_{oc} depends on the redox potential of the mediator halide ion and conduction band of the perovskite.

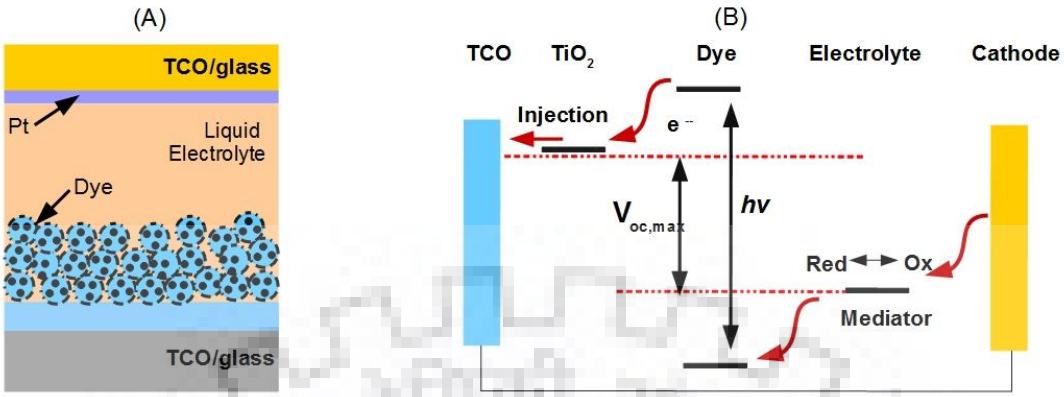

Figure 2.12: (a) Liquide electrolyte DSSC structure (b) Mechanism of charge flow in liquid electrolyte DSSC

2. **Solid-state mesoscopic structure**

This was a first alternative to liquid electrolyte to overcome instability issue. Solid Hole Transporting Material (HTM) used was Spiro-MeOTAD. The device configuration as shown in **figure (2.13)** was given the name as mesoscopic structure since it uses mp-TiO_2 layer. The mp-TiO_2 layer thickness was 0.6 µm which reduces the material usage. HTM makes direct contact to the perovskite sensitizers by penetrating from the pores of mp-TiO_2 and prevent the shunting of Electron Transporting Material (ETM) and back contact electrode by covering as a capping layer.

V_{oc} of these devices increased from 0.7 V to 0.89 V, because of well arrangement of HOMO (Highest Occupied Molecular Orbital) of Spiro-MeOTAD and valance band of the perovskite, which resulted in more efficient hole extraction compared to conventional device structure. It has also shown better device stability.

3. Meso-super-structured structure

It resembles to the mesoscopic structure but differed by two things, one is insulating metal oxide like Al_2O_3 instead of mp-TiO_2 and second is extremely thin layer of absorber (ETA) on the surface of porous Al_2O_3.

Some devices with mixed halide perovskite and Al_2O_3 layer achieved significantly higher V_{oc} values. Which indicates that the mixed halide perovskites has larger carrier diffusion length and less non radiative recombination.

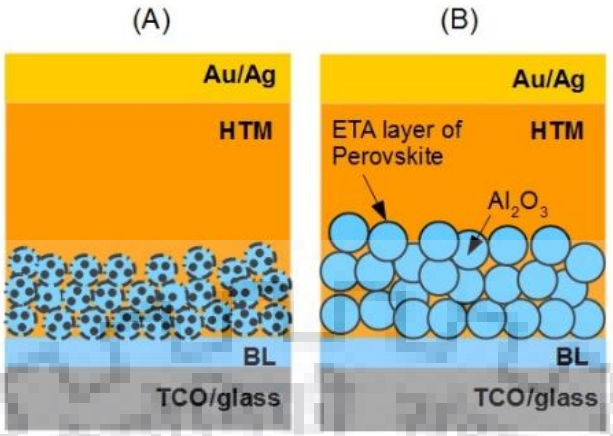

Figure 2.13: (a) Solid-state mesoscopic structure (b) Meso-super structure

Here, charge transport mechanism is different than the mesoscopic structure because the electron transport from perovskite to the Al_2O_3 is energetically unfavourable. Which is attributed to lower conduction band of $MAPbI_{3-x}Cl_x$ with respect to aluminium oxide [17, 18]. It concluded that, the mesoscopic scaffold is not required for transporting the electron from perovskite to the c-TiO_2. It is because of long diffusion length of carriers in the perovskite [19, 20]. Snaith et. al. removed the mesoscopic scaffold and came with planar junction device with PCE of ~ 1.8% as his preliminary device.

4. Regular structure

When exciting opto-electronic properties of the perovskites were explored like low traps with large diffusion length of carriers. Which indicated to use thicker film of the perovskite instead of the ETA, so that it can improve the photon absorption and prevent shunting between electrodes. As a result regular structure was advanced on meso-super structure but through a dense and thicker layer of perovskite. It gained huge success all around the globe due to its higher efficiency.

In 2013, Hoe et al. reported 12% PCE with pillars of $MAPbI_3$ on top of completely filled pores of mp-TiO_2. Later, Burschka et al. did optimisation of thicknesses of different layers, which exhibited PCE of ~ 15% [14]. They fabricated thin perovskite layer with 50 nm thickness above mp-TiO_2 layer with ~ 300 nm thickness. Later, with this architecture PCE of 17% achieved through 150 nm thick layer of perovskite and PCE of 19.3% through 300 nm thick perovskite layer [21, 22].

5. Planar structure (n-i-p)

This is quite simple configuration of PSCs. As the mesoscopic scaffold is not participating to electron transport, removal of mesoporous oxide layer from regular structure leads to planar structure. This structure has two heterojunctions, one is in between n-type ETM and intrinsic

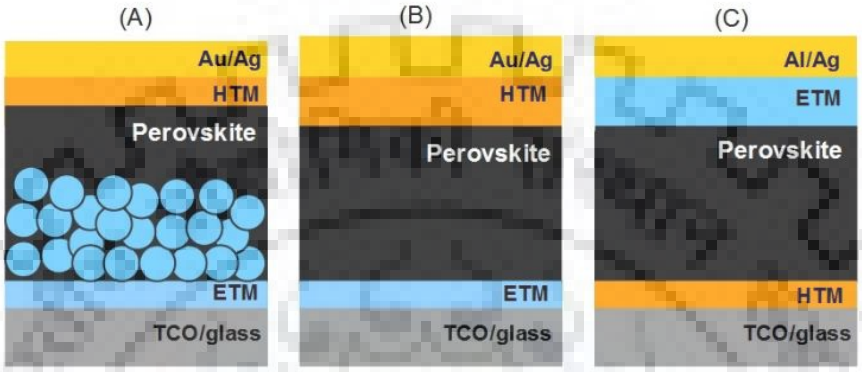

Figure 2.14: (a) Regular structure (b) Planar structure (n-i-p) (c) Inverted structure (p-i-n)

perovskite layer while other one is in between intrinsic perovskite and p-type HTM. Therefore it is also called as n-i-p structure. The structure consist of TCO\ETM\Perovskite\HTM\Metal anode as shown in **figure (2.14)**.

First attempt made by Snaith et al. with mixed halide perovskite resulted in 1.8% PCE, likely due to incomplete film coverage . Later, in 2013 optimizing the processing condition improvement in PCE was noted and in 2014 PCE of 11.4% was achieved but still the film was porous and had high surface defect density [23]. With the help of advancement in deposition technique and co-evaporation method for film making further, enhancement in the efficiency was achieved. This devices has shown highly stable performance over hundreds of hours in operating conditions which makes it promising candidate for commercialization.

6. Inverted planar structure (p-i-n)

It is stated as an inverted structure because it has p-type–intrinsic-n-type hetero-junction structure compared to regular and n-type-intrinsic-p-type planar structure. This architecture is widely used in organic photovoltaic. It has TCO\HTM\Perovskite\ETM\ Metal cathode layers as shown in **figure (2.15)**.

At the initial stage of development PEDOT:PSS (poly-polystyrene sulfonate) was used in HTM and bathocuproin (BCP) used as ETM. So the device configuration was like ITO\PEDOT:PSS\$MAPbI_3$\$C_{60}$\BCP\Al, which yielded PCE of 1.6% [24]. Replacing the C_{60} with $PC_{61}BM$ (phenyl-C61-butyric acid methyl ester) enhancement in the PCE was noticed up to 3.9%.

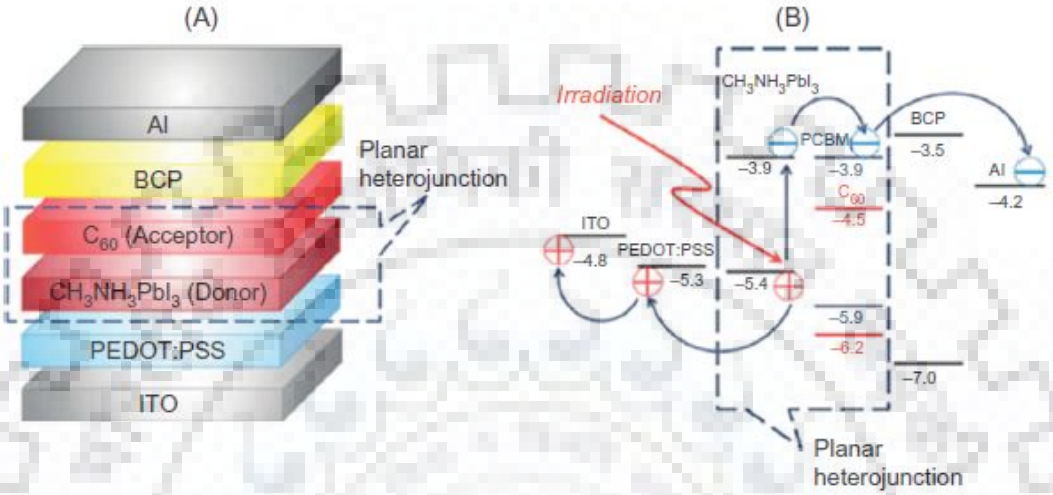

Figure 2.15: (a) Inverted device structure (b) Energy level diagram in inverted perovskite solar cell [40]

Snaith et al. reported PCE of 9.8% with FTO\PEDOT:PSS\$MAPbI_{3-x}Cl_x$\$PC_{61}BM$\$TiO_x$\Al layered structure [25]. You et al. optimised deposition and got 11.5% efficiency [26]. With device architecture improvement in the efficiency was very fast. Device with larger grain perovskite got efficiency of 19.5%. These devices has exhibited better ambient stability also.

2.5.3: Working principle

At the initial stage of development of the PSCs, the working mechanism of the PSC was not known exactly, so according to earlier hypothesis two charge selective interfaces are required. Those interfaces are perovskite\ETL and perovskite\HTL which are electron selective and hole selective interfaces respectively. Where, ETL is electron selective material while HTL is hole selective material due to their affinity towards the selective charge carrier. The **figure (2.16)** depicts various HTL, ETL used with various perovskites.

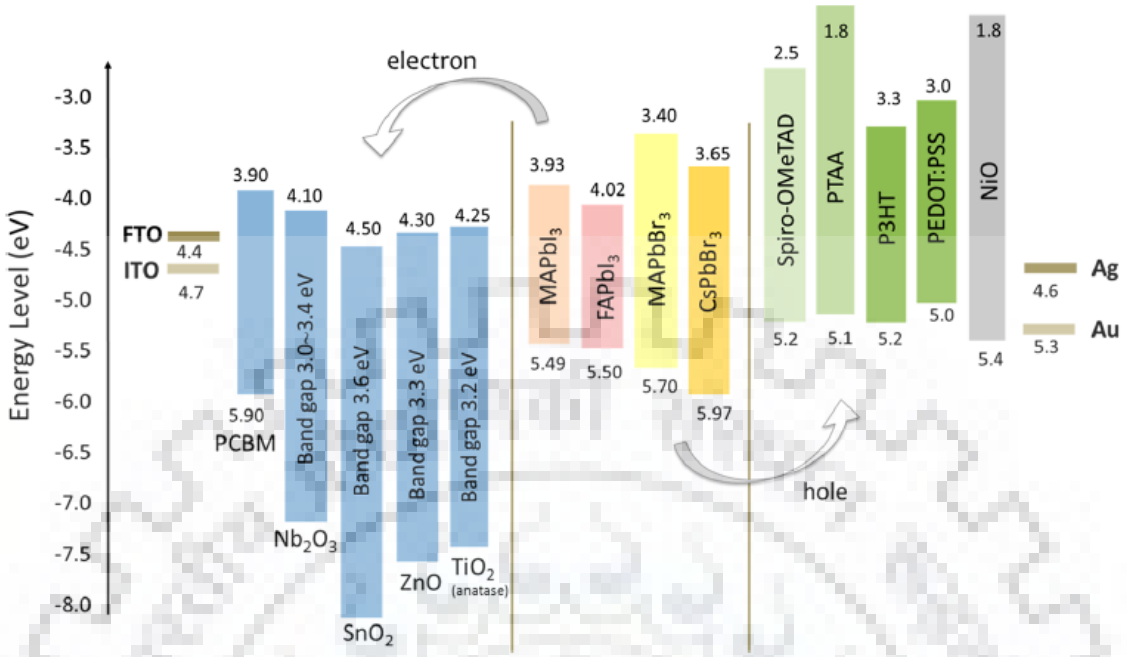

Figure 2.16: Energy level diagram of various absorbers, ETMs, HTMs, TCOs and electrodes.[2]

Later, as the perovskite material's exciting opto-electronic properties were discovered the conclusion came that the interfaces are not required to dissociate the generated excitons (electron-hole pair). As the exciton binding energy for perovskite material is quite low (tens of meV) and comparable to thermal energy under operation, so these excitons can dissociates without interface i.e. inside the perovskite itself. The large diffusion length and adequate mobility of charge carriers makes it possible to diffuse to the respective electrode if used with optimised thickness of perovskite. [27]

PSCs are heterojunction devices so the built in potential is created due to difference in the work potential of different materials at the two interfaces. When solar radiation hits the cell, the photon is being absorbed by the Perovskite material and excitons are generated. In consequence of longer diffusion length of the charge carriers for perovskite material, they will diffuse to respective interfaces and gets transferred towards the electrode as shown in the **figure (2.16)**.

2.6: Major challenges for perovskite solar cells

The potential of PSCs has been enhanced from 3.8 % to 23.7% in less than a decade. Although, rapid progress in the cell efficiency of perovskite solar cells, it is still facing issue of the moisture persuaded instability, thermal instability and hysteresis behavior [18, 19]. Organic inorganic halide like $MAPbX_3$ has the limitation in practical use because its hygroscopic nature and also the lead is showing toxicity, which is not good for environment.

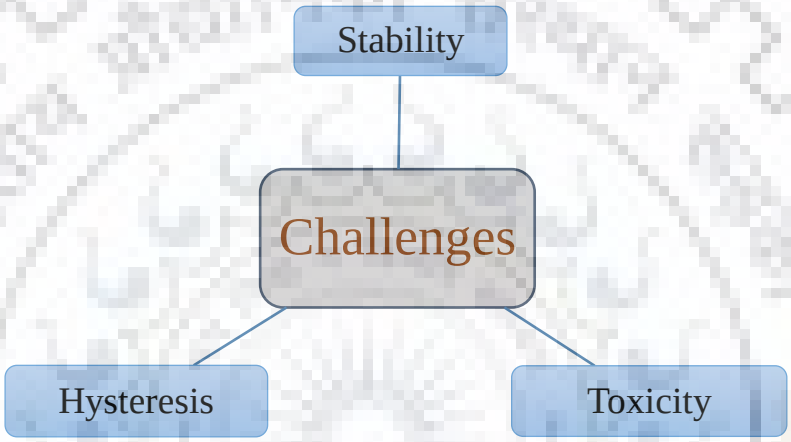

Figure 2.17: Challenges for perovskite solar cells

2.6.1: Stability

Here, Stability means nearly unaltered long-term ability to produce power from solar radiation .

In the starting phase of development there was not any standard long-term characterization methods but in recent year's reports of some standard characterization have been published.

Crystal structure stability is mainly important because it got affected by temperature and pressure. The structure of perovskite material affects the optoelectronic properties of the material, which is of more concern in solar cell application. As the perfect perovskite structure has tolerance factor (t) = 1 which is cubic perovskite. Poorer tolerance factor introduces the shift in the structure from orthorhombic/tetragonal and less symmetry, which brings on undesirable consequence on optoelectronic properties of perovskite.

The solar cell has operating temperature range from -40 °C to 85 °C. $MAPbI_3$ is showing tetragonal structure at room temperature, While during cooling, it is showing cubic phase shifts to tetragonal around at 55 °C that is not good for performance [28, 29]. Thermal coefficient of expansion of the standard perovskite is approximately 1.5×10^{-4} K^{-1}, which is very high compared to glass, CdTe and CIGS, so it affects the mechanical stability of the device due to temperature cycling [30].

$FAPbI_3$ has better thermal stability compared to $MAPbI_3$ perovskite because the phase transition temperature of 150 °C [31]. While the problem with the $FAPbI_3$ is unstable under moisture. To improve the stability of $FAPbI_3$ under the moisture replacing the 10% of organic FA cation with Cs cation which also improves the phot-stability. Lattice contraction takes place due to incorporation of Cs ion, as the size of Cs ion less compared to the FA cation which lowers down the tolerance factor [32].

Many research work has shown that the perovskite material is showing instability under environmental factors like **Moisture**, **Thermal**, **Oxygen** and **UV**.

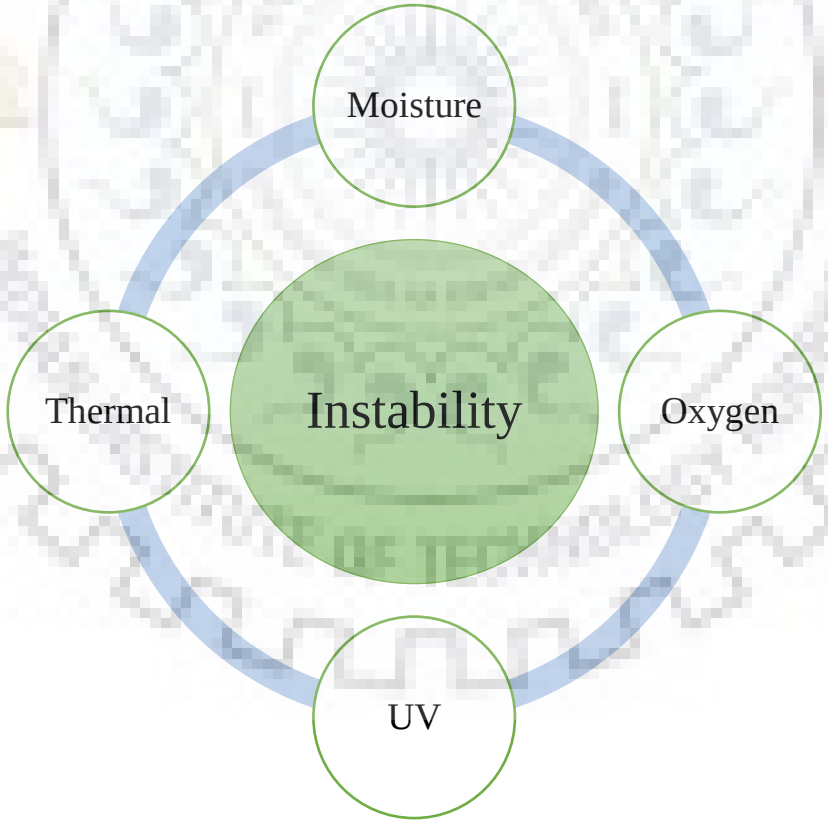

Figure 2.18: Factors affecting the stability of perovskite materials

$MAPbI_3$ is highly sensitive to the moisture that it gets hydrolysed in the presence of moisture. It gets decomposed even if a single molecule of water reacts with it, this was studied by the Walsh and co-workers [11]. They projected that single water molecule will mingle with $MAPbI_3$ by extracting one proton from ammonium and converting the perovskite in to an intermediate hydrate form, which then converted to HI, CH_3NH_2, PbI_2, and with that releases the water molecule and cycle continues as shown in **figure (2.19)** [11].

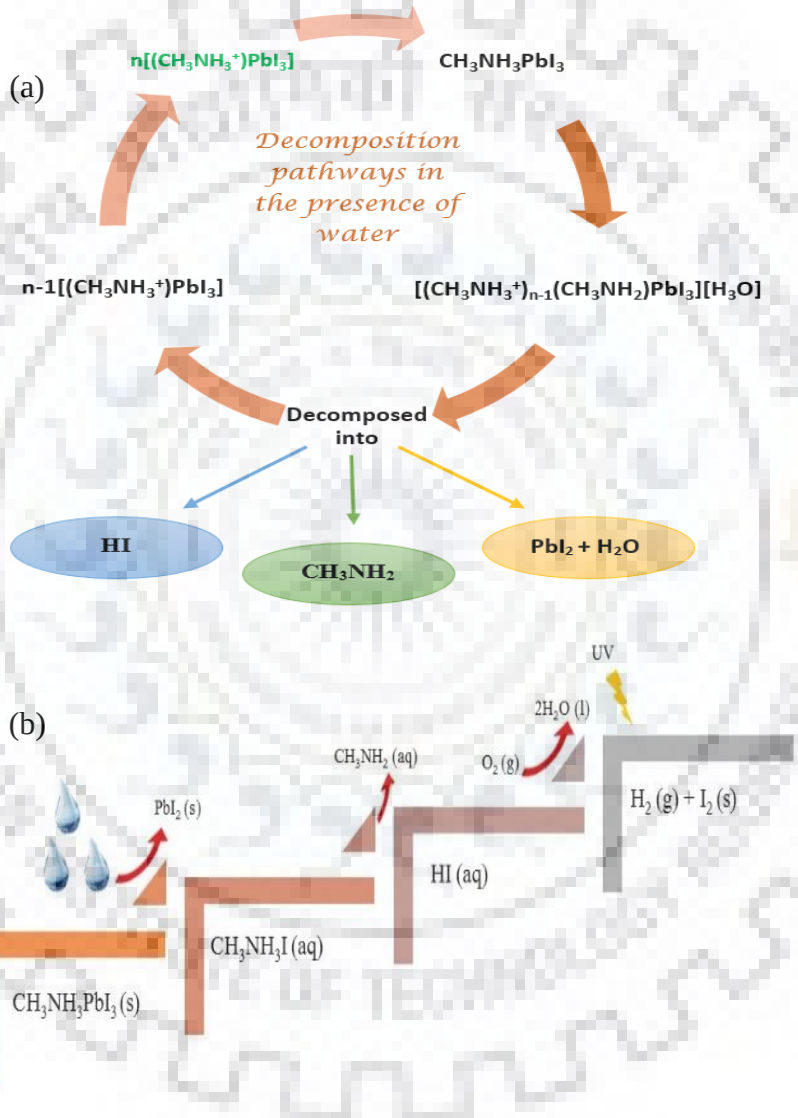

Figure 2.19: (a) Decomposition pathways in presence of water (b) Cumulative effect of humidity, UV and Oxygen. [11]

Niu et al. has studied the integrated effect of Moisture, Oxygen and UV light on the perovskite layer as time passes [33]. Above certain moisture level, the MAI will start dissolving and inorganic

halide will remain in the structure. Oxygen and photon helps in this irreversible decomposition to takes place. Oxygen itself couldn't trigger the perovskite decomposition, so it is advisable to store perovskite in dry and dark environment. Degradation of perovskite material with humidity and temperature could be more severe. Some studies have shown that the high relative humidity will enlarge the crystal size of perovskite and improved connection amid crystals through two-step fabrication. Relative humidity (RH) at the time of fabrication of perovskite layer has effect on the performance, so it should be at the optimal level. Cronin, H.M. et al. have shown their best device fabricated under 20% RH and 45 min post-annealing process. The moisture at the time of fabrication has offered additional solubility of organic precursor with decrease in PCE has observed with less than 5% after some days in ambient atmosphere [34, 35].

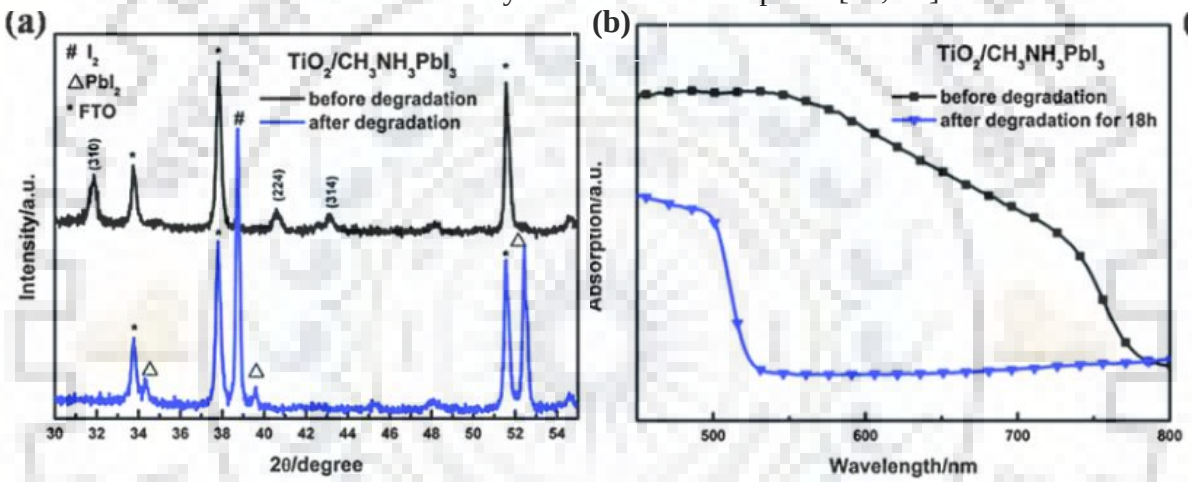

Figure 2.20: (a) X-ray diffraction pattern for $MAPbI_3/TiO_2$ before and after degradation (b) UV-visible spectroscopy of $MAPbI_3/TiO_2$ before and after degradation (degradation time is 18hr and humidity of 60% at 35 °C) [34]

Photocatalytic degradation takes place due to long-time exposure of perovskite under UV light. To reduce this effects use of FTO conducting glass support and compact TiO_2 or SnO_2 layers which filters out UV photons is advantageous. Nam-Gyu Park et al. also suggested that use of mixed halide or lower dimensional perovskites are potential paths to improve the stability of perovskite layer. It can be also achieved by the suppression of chemically liable organic cation [36].

As the $MAPbI_3$ is made up of lead halide and organic halide, the lead halide part exhibit photo-decomposition. PbI_2 has bandgap of around 2.47 eV, which falls under visible spectrum. It absorb the visible photons to create electron-hole pair, electrons could be trapped on Pb^{+2} and that can

reduce it into Pb, driving to decomposition of PbI_2. If the PbI_2 amount is in excess by small fraction then it drive to detorioration of perovskite under visible light even in the inert atmosphere [30].

When perovskites are exposed to e-beam with higher energy than the solar-photon it shows degradation due to heating effect [30]. In $MAPbI_3$, $CH_3NH_3^+$ move to top surface and get reduced to CH_3NH_2 upon scanning with elelctron beam, CH_3NH_2 will be removed from the surface of the film due to high vacuum that results in reduction in the thickness of the film [30]. It can be also seen as e-beam persuaded creation of vacancies, defects and directional ion migration in perovskite. [30]

$MAPbI_3$ is also get affected by the low energy electrons because it affects the chemical and structural properties. Generation of gases like HI and NH_3 with the formation of polymer hydrocarbon residue ($-CH_2-$) and PbI_2 takes place when electrons attacks to organic part of the perovskite and breaks the C-N bond in $CH_3NH_3^+$[30].

2.6.2: J-V hysteresis

This is witnessed when the altered voltage sweeping rate in addition with direction is applied to the cell [37].

Two types of hysteresis are observed:

Normal hysteresis: It shows higher efficiency when voltage is decreases (reverse scan) but lower efficiency when voltage is increased (forward scan).

Inverted hysteresis: It is shwoing opposite behaviour than normal hysteresis.

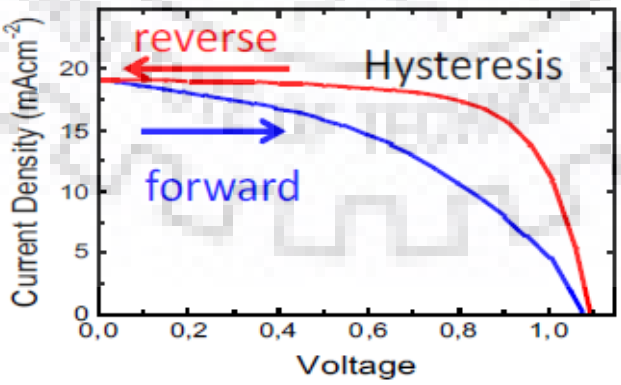

Figure 2.21: Hysteresis in J-V measurement

It is difficult to say about exact Mechanism of hysteresis but in recent studies numerous concepts had been proposed like ion migration, ferroelectric polarization, capacitive effects and charge trapping [38].

To get the exact performance of the solar cell I-V characteristics has to be calculated for that the voltage sweeping rate is applied to the cell and maximum power point is to be found. In PSC, I-V curve changes depending on how fast the scanning voltage is being varied and the direction of scan. Ultimately hysteresis puts challenge on the correct measurement of PCE and so as to stability.

2.6.3: Toxicity

The noxiousness in the perovskite layer originates due to lead cation of the $MAPbX_3$. As known already that the lead is harmful for the environment so the issue of lead use in perovskite is appeared on commercialization of PSCs.

First tin was studied as the substitute of the lead in the perovskite as $MASnI_3$, but the problem with Sn was it easily gets oxidized from Sn^{+2} to Sn^{+4}. Tin based devices has exhibited weak device performance [39]. Later some research work showed that, the using hybrid Sn-Pb metal cation in the perovskite as $MASn_{1-x}Pb_xI_3$ has shown good results like PCE of 15.2% with less toxic effects than the $MAPbI_3$ [40].

Bismuth, who is neighbour to Pb was the next potential candidate. It formed stable $(MA)_3Bi_3I_9$ (MABI) perovskite material. It has exhibited appreciable stability for 1000 h under ambient conditions [41]. The problem with the Bi-based perovskite is that it shows less PCE, low V_{oc} and extremely low J_{sc}. So further research on Bi-based perovskite material is carried out like $(MA)_2KBiCl_6$ and Cs_2AgBiX_6 with different halides but none of the work has exhibited promising results.

Various kinds of lead-free active material like $MAGeX_3$, $CsGeI_3$, $MASrI_3$, $MACaI_3$ has been investigated but not a single one has shown better performance as compared to lead based PSCs.

2.7: Advancements in the perovskite materials for stability

2.7.1: Hybrid halide anion:

The Photo-physics of perovskite material tells that the electronic structure depends on the p orbit of lead and halide, so for controlling the bandgap of the $MAPbI_3$ mixture of the halides can be used.

The first mixed halide PSCs of I/Br was reported by Noh. et al. with efficiency of 12.3% under standard AM 1.5 illumination. In this work, they are claiming that bandgap can be modified to utilize entire visible spectrum by changing I/Br content in the $MAPbI_{3-x}Br_x$. As the Br content increases the bandgap increases also the humidity shelf-life stability (for Br content >20%) but for getting good initial efficiency the Br content should be less than 10% [42].

$MAPbI_{3-x}Cl_x$ is studied extensively as a mixed halide perovskite. Stranks et al. showed that the diffusion length of charge carrier was more than 1 micron for this kind of mixed halide perovskite, where chlorine plays an important role for stability and conductivity of perovskite [19].

Triple halide anion perovskite $MAPb(I/Br/Cl)_3$ was first studied by B. Suarez et al., they have explained the recombination characteristics as a function of halide content in the perovskite. They observed that charge recombination reduced due as Br/I content increases. The charge recombination rate has been reduced due to incorporation of the Cl and Br, at the same time stability is also improved that all the devices were showing the 80% of initial performance even 1 month after preparation [43].

2.7.2: Hybrid A cation

A cation site of the perovskite material doesn't participate directly to the energy band structure. The size of the A cation will alter the B-X bond length which in turn affect the energy band structure of the perovskite. Larger the size of A cation smaller the bond length of B-X and less will be the energy bandgap. Anna Amat et al. has demonstrated the effect of different cations on perovskite structure [44].

$(MA)_x(FA)_{1-x}PbI_3$ as an active layer was the first mixed A cation solar cell that was reported by Pellet et al. [45] which showed the band gap tunability by varying the composition of MA and FA cations. It has observed that at x=0.6 resulted in highest PCE of 14.52%. Y Deng et al. [46] reported

that $(MA)_x(FA)_{1-x}PbI_3$ perovskite synthesised with the doctor blade coating method has shown PCE greater than 18% and stability more than 20 - 30 days in air. It also conclude that as FA/MA ration increases the absorption edge shows redshift.

Stability issue is because of MA organic cation. Therefore, various efforts to replace A site organic cation with inorganic cation leads to better stability with compromising the efficiency.

Initially, $Cs_x(MA)_{1-x}PbI_3$ as an active layer of perovskite solar cell with inverted structure achieved PCE of 7.68% [47] in later studies optimised value for the same perovskite but with regular structure for x = 0.09 achieved 18.1% efficiency [48]. Rb is also considered as the potential candidate to enhance the stability and efficiency for the mixed A cation like $(FA/Rb)PbI_3$ perovskite solar cell.

2.7.3: Simultaneous mixed site ions

As perovskite has general form of ABX_3, it is possible to study many possibilities with mixing of elements for different sites like A cation, B cation and X halide anion. Among various mixture still lead based mix perovskite has higher efficiency.

Table 2.5: Combination of A, B and X site ions

A cation	B cation	X anion
MA, FA, Cs, Rb, K	Pb, Sn, Bi, Ge, In	Cl, I, Br

Formamidinium lead triiodide ($FAPbI_3$) is not stable at room temperature i.e. it changes its phase from α-phase (black) to δ-phase (yellow) that is undesirable, to overcome this problem Zheng et al. suggested the alloying of MABr. Alloying caused the perovskite lattice to contract which balances the lattice strain. $FAPbI_3$-MABr solar cell fabricated has exhibited improved stability under humid air of ~ 50% RH and 23 °C [49].

$CsPbI_2Br$ mixed halide perovskite contains benefits of small bandgap of $CsPbI_3$ and good stability of $CsPbBr_3$ perovskite. To improve further these properties, it should be doped with potassium as suggested by Nam et al. [50], $Cs_{0.925}K_{0.075}PbI_2Br$ was reported with champion device PCE of 10% and average PCE of 9.1% with extended air stability.

2.7.4: Low dimensional perovskites

The parameters of device fabrication like film morphology, uniform film coverage and grain size plays vital role for device performance. Many improvements in device fabrication has led to enhanced efficiency but still the fabrication and characterization has to be carried out in controlled atmosphere because of the stability issue of the perovskite in ambient condition. Still, the attempts to enhance the efficiency with the stability in environment were complement by synthesis of new stable materials.

Currently the development of lower dimensional (LD) perovskite materials has been increased to explore their photonic and opto-electronic properties which can help to stability of solar cell. The materials having their one dimension in nanoscale range are called as Low-dimensional materials. These materials shows quantum confinement due to which exhibits unique properties like tunable opto-electronic properties and mechanical flexibility. LD perovskites can be prepared to have different morphology like zero-dimensional, one-dimensional, two-dimensional as Quantum dot, Nano-rod, Nano-sheets respectively.

Slicing off the 3D perovskite will results in sandwich like layered perovskite called quasi-2D or 2D perovskite, again slicing off the 2D perovskite will be end as single chain like 1D perovskite. When large A cation (generally long organic) is used which cannot fit into the cubic void created by the octahedral framework, will be acting as a capping or barrier to the 3D perovskite and results in layered structure.

Quasi-2D perovskite has general structure formula $(R)_2(A)_{n-1}B_nX_{3n+1}$, where R is large organic molecule cation, A is organic or inorganic cation, B is divalent metal cation, X is halide anion, and n represent number of layers of octahedral unit. When $n = \infty$, it represent 3D perovskite with ABX_3 structure, n = 1 means that 2D structure, n = 2 is for bilayer perovskite i.e. two BX_6 octahedra thick similarly for n = 3, 4 and so on.

DFT simulations has shown that moving from 3D to 2D or 1D increases the formation energy which led to increase in the stability [51]. Reduction in the dimensionality of inorganic perovskite causes enhancement in exciton binding energy and widening of the bandgap [51, 52].

In a mixed Rudlesden Popper phase, larger organic cation such as 2-phenylethylammonium, and octylammonium, butylammonium, 1,4-diaminobutane etc. increases the hydrophobicity of

perovskite layer which prevents the diffusion of water molecule, and introduces van der waals forces between adjacent layers. This determines the stability of the perovskite films.

If the tolerance factor is greater than unity imply that the formation of layered structure. It is possible to have different oriented layers such as <0 0 1>, <0 1 1>, and <1 1 1>. The number of sheets inside the organic cation capping is controlled by the proper ration of organic cation while the organic molecule chosen decides the crystallographic orientation of the inorganic network.

Synthesis of 2D perovskite by solution processed technique include one step and two step method.

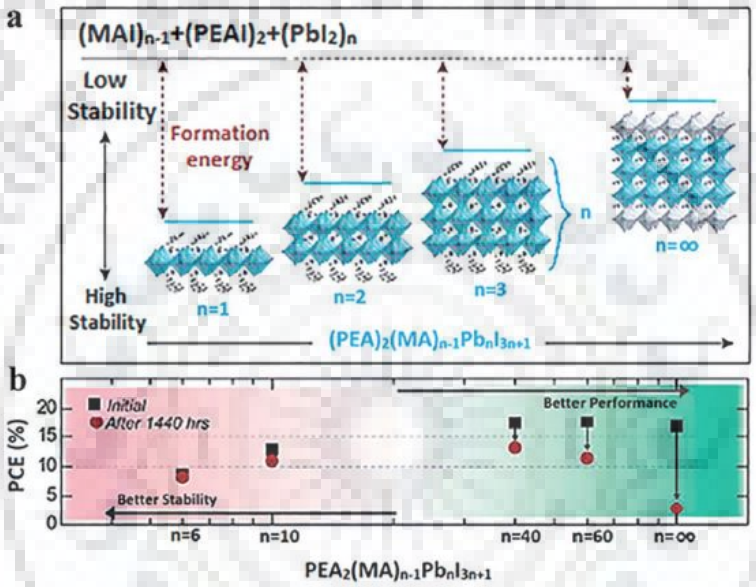

Figure 2.22: (a) Relationship between dimensionality and stability/formation energy of perovskite [$(PEA)_2(MA)_{n-1}Pb_nI_{3n+1}$] (b) PCE of dimensional perovskite [52]

It is same as the 3D perovskite synthesis but with modified precursor stoichiometric ratio. The precursors in proper stoichiometric ratio are dissolved in solvent and deposited by spin-coating on substrate. For the preparation of the 2D perovskites molar ratio of long organic cation to lead halide is 2:1.

- **2D perovskites as an absorber:**

Layered perovskites have tunable properties and good stability, so they were introduced in PSCs. Smith et al. [52] presented 2D hybrid perovskite as an active layer, for the first time in PSC devices. They used tri-layered structure of Pb-I framework which is separated by large organic cation PEA (Phenethylamine) i.e. n = 3 in structural formula $(PEA)_2(MA)_{n-1}Pb_nI_{3n+1}$. They also showed that 2D perovskite has better humidity resistance than the $MAPbI_3$. In humid environment with RH =

52%, MA based 3D perovskite decomposes within 4 to 5 days where as 2D perovskite film exhibited no substantial changes within time span of 46 days. The devices of this 2D perovskites has low efficiency around 4.73% due to suppression of out-of-plane charge transport by PEA [52].

To improve the PCE of 2D perovskite devices, mixture of 3D and 2D was investigated by Yao et al. [53] by two-step method. First spin-coating of the compact PbI_2 and PEI·HI (Polyethylenimine hydroiodide) followed by coating of MAI layer. They fabricated devices with different molar ratio of 2D/3D mixture i.e. $(MAPbI_3)_{1-x}[(PEI)_2PbI_4]x$. The device with x = 2% of 2D perovskite mixture has shown the best PCE of above 15% with higher moisture stability compared to $MAPbI_3$. $MAPbI_3$ got degraded after 120h of operation in RH = 50% while PCE of mixed 2D/3D perovskite $(MAPbI_3)_{1-x}[(PEI)_2PbI_4]_x$ with x = 2% molar ratio drecreased by 8% on 14^{th} day.

Cao et al. [54] used small organic cation n-butylamine (BA) to fabricate 2D perovskite films of structural formula $(BA)_2MA_2Pb_3I_{10}$. They have noticed that the degradation of 2D perovskite film doesn't takes place even after 2 months exposure under 40% RH. Devices of this 2D films has PCE less than 5% due to poor charge transport and absorption.

Quan et al. [51] fabricated $(PEA)_2MA_{n-1}Pb_nI_{3n+1}$ with different n values and concluded that the n = 6 is showing highest stability but the PCE is lowest which is attributed to its poor mobility. LD devices shows better thermal and moisture stability compared to 3D ones.

To study the type and size effect of the organic cation on the layered structure, safdari et al. [55] synthesized pure 2D perovskites with different organic chain. They proposed that the larger cation is not preferred for 2D PSCs, still the PCE is remained as a challenge. Introduction of bulkier cation helps to reducing the dimensionality but they act as an insulator, which hinders the charge transport and reduces the electrical conductivity. It was observed that the $MAPBI_3$ has approximately hundred times higher electrical conductivity than the 1D $(CH_3CH_2NH_3)PbI_3$ perovskite.

In the direction of improvement in the charge transport in layered perovskite, Tsai et al. [56] came with hot casting method for orienting the planes of layered perovskites towards single crystalline. The crystalline planes are aligned out-of-plane to have better charge transport. Here, they have prepared $(BA)_2MA_2Pb_4I_{13}$ which resulted in device with PCE of 12.52% with quite higher humidity and moisture stability.

Later, Chen et al. [57] has replaced linear chain of butylamine with short branched molecule iso-butlamine (iso-BA). They prepared films of 2D perovskites via room temperature and hot casting process. Room temperature synthesized film exhibited the significantly increased mobility and charge extraction along with improved crystallinity and out-of-plane orientation.

To study the doping effect of the layered structure 5% Cs was introduced in 2D layered $(BA)_2Cs_{3x}MA_{3-3x}Pb_4I_{13}$ lattice. PCE of these cells were improved from 12.3% to 13.7% with excellent enhancement in thermal and moisture stability. These cells retained 89% of initial efficiency after 1400 hrs under RH of 30% while un-doped 2D perovskite retained 74% of its initial PCE. It was concluded that Cs doped devices have more hydrophobic surface and stable phase structure [58].

Using the crystallographic orientation strategy, vertically oriented 2D perovskites can be grown that was demonstrated by Zhang et al. [59], which improved the PCE and stability of the device. They synthesized vertically oriented $(BA)_2MA_2Pb_3I_{10}$ which exhibited average PCE of 6.82%.

Apart from small organic molecules polymers cation have been also studied, which prevent moisture diffusion. Polyethylenimine (PEI) was used as the polymeric organic cation to form $(PEI)_2(MA)_{n-1}Pb_nI_{3n+1}$ 2D perovskite with n = 3, 5 and 7 by Yao et al. The device with n = 7 has shown the efficiency of 10.08% which is better than BA based 2D perovskite. Owing to this polymeric-ammonium cation charge transport properties has been improved. $MAPbI_3$ devices exhibits immediate degradation when exposed to 50% humidity, while for PEI based 2D perovskite has shown no significant changes observed even after one month [60].

Gan et al., demonstrated pinhole-free and homogeneous 2D perovskite film synthesis under ambient conditions. They used TiO_2 nanorods to have better contact and coverage of film. The champion device of $(PEA)_2MA_2Pb_3I_{10}$ showed 3.72% efficiency and stability under 60% RH in dark for 60 days [61].

One-year stable perovskite devices were fabricated by mixing of AVAI ($HOOC(CH_2)_4NH_3I$), MAI, and PbI_2 precursors to prepare ultra-stable 2D/3D perovskite. The device containing 2D/3D perovskite/organic HTM/Au boughten PCE of 14.6% while the carbon electrode based HTM free configuration has showed PCE of 11.2% for 100 cm^2 module. The 2D/3D perovskite with Spiro-OMeTAD as HTM and gold electrode reserved 60% of initial PCE after 300 hrs of operation under

argon atmosphere while 3D perovskite retained 40% of initial PCE. Extraordinarily, 2D/3D mixed perovskite without HTM and with carbon as a contact electrode showed stability under operation at 55 ºC for more than 10,000 hrs [62].

Iagher and Etgar investigated the effect of the Cs and concluded that the introducing Cs in 2D/3D perovskite can improve PCE but stability affected inversely. Further, they explored new organic molecules like cyclohexylammonium iodide (CHMA), and benzylammonium iodide in 2D/3D perovskite. They commented that the benzylammonium iodide based 2D/3D perovskite reserved 55% of its initial PCE under 30% - 50% RH and 50 ºC - 60 ºC temperature condition which is far better than BA/Cs based 2D/3D devices. The poor stability of Cs and MA based absorber layer is due to difference in ionic radii causes strain and distortion in the structure [63].

- **2D perovskites as a capping layer:**

The stability issue motivated researchers to concentrate more on the low dimensional perovskites as possible solution due to its moisture resistance property. LD perovskite not only be used as absorber layer but also as capping layer or interface layer to enhance stability by protecting the absorber layer. It was suggested that the interfacial layer of 2D perovskite can act as protecting layer for perovskite absorber and at the same time improving the charge transfer through bandgap matching.

In this regard, PEI·HI was used to form 2D perovskite $(PEI)_2PbI_4$ as interfacial layer for protection of perovskite film. The device with capping of $MAPbI_3$ showed 13.09% efficiency and 10 days stability under illumination at 50% RH [53].

Hu et al. conveyed that using heterojunction of $MAPbI_3$/layered perovskite in the device can lead to efficient light absorption and moisture resistance. Incorporating layered structure based on MA, PEA or BA on top of $MAPbI_3$ exhibits improved performance. $MAPbI_3$ based devices showed 70% retention of initial PCE while heterojunction devices showed decrease in PCE from 12.5% to 11.5% under device stability test at 75% RH and room temperature for 19 days.

CHAPTER 3: Experimental procedures

3.1: Aim

Improving the ambient stability of methylammonium lead iodide ($MAPbI_3$) solar cell using organic pseudohalide ligand as an additive.

3.2: Materials and methods

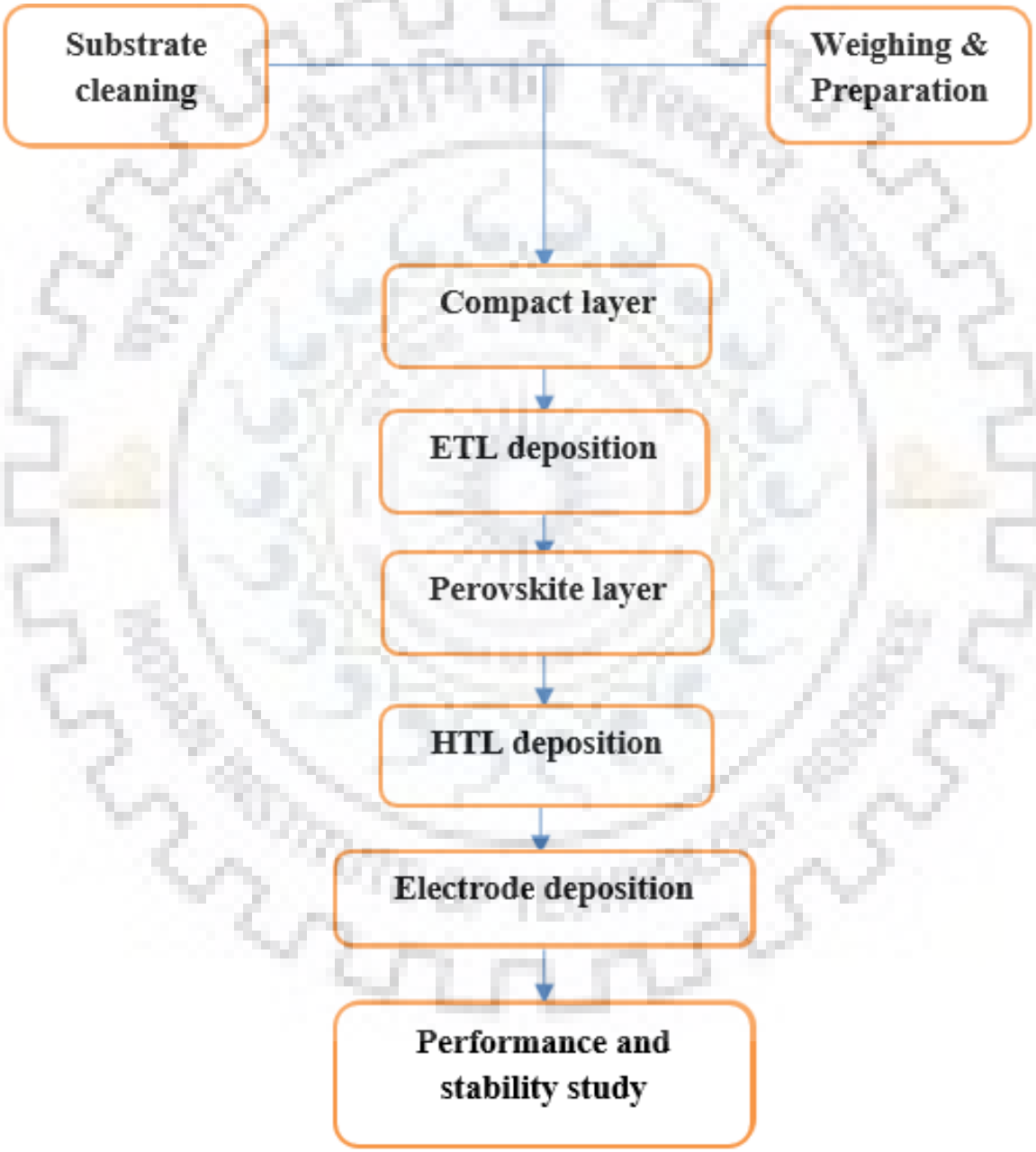

Figure 3.1: Experimental methodogy

3.2.1: Substrate preparation:

The glass/FTO were cut in square size of 1.5 cm× 1.5 cm. These square substrates were kept in a beaker with stand, then processed with different solutions

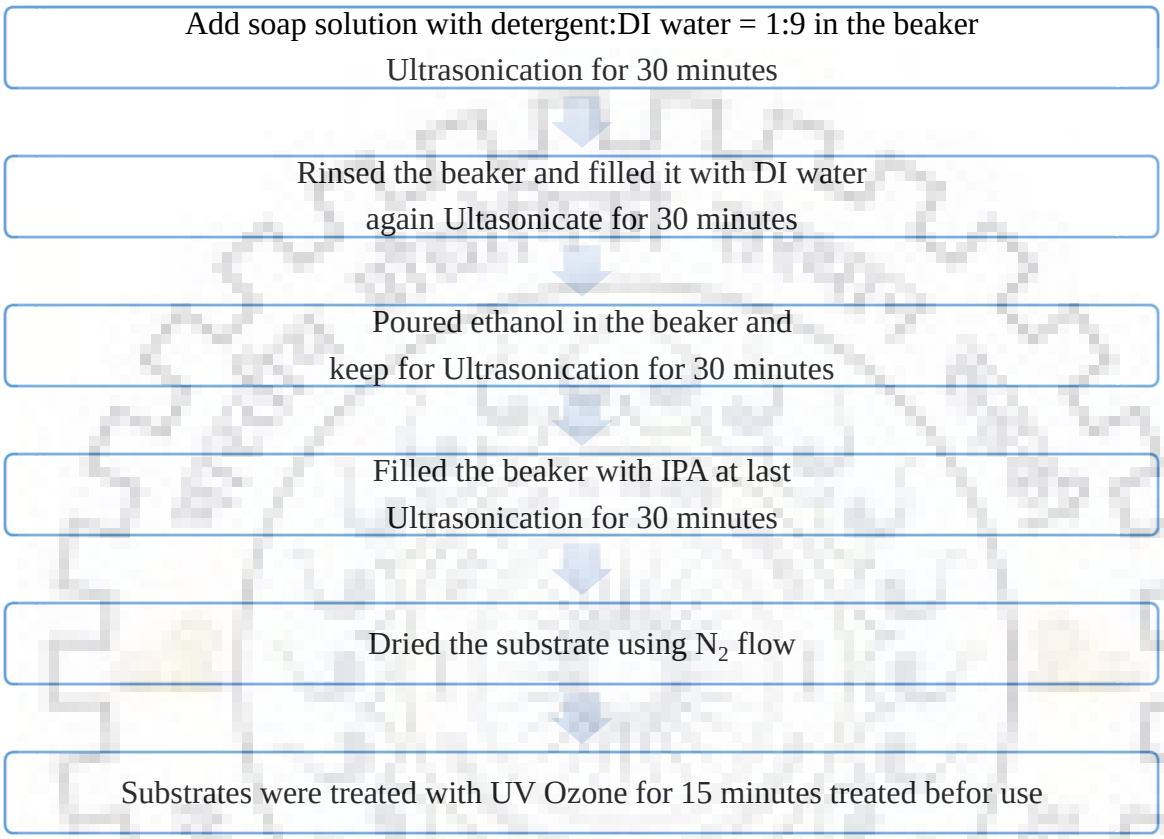

Figure 3.2: Steps for substrates cleaning

3.2.2: Material requirement for film and its fabrication:

Materials that are used to prepare the films and devices are listed in the table with their respective quantity. These amount is calculated based on 1.4 molar solution in 600 µl DMF. Here, quasi-3D perovskite has formula $(R)_2(MA)_{n-1}Pb_nX_{3n+1}$ with different n values which depends on relative molar ratio of components added. R represents organic phenylethylammonium cation (PEA^+) and X represents mixture of iodide anion (I^-) and pseudohalide anion (SCN^-). So,organic ligand used is phenylethylammonium thiocyanate (PEA(SCN)).

Table 3.1: Material requirement

Solution of	MAI (mg)	PbI_2 (mg)	PEA(SCN)
$MAPbI_3$	133.534	387.240	-
n = 80	131.864	387.240	3.765
n = 60	131.244	387.240	4.948
n = 40	130.195	387.240	7.530

1. **Compact layer (CL) preparation:**

Using acetone rinsed and dried 5 ml vial and magnetic stirrer, compact solution was prepared as described. Added 5 ml of 2-Methoxyethanol and stirred at 200 rpm, followed by very slow dropwise addition of 0.767 ml Titanium butoxide to prevent precipitation. The solution for stirring for 5 minutes and then 0.230 ml of Acetylacetone was mixed. Using proper covering with aluminium foil, the solution was kept for overnight stirring at room temperature.

- **Compact layer deposition:**

The prepared compact TiO_2 solution is spin coated on the UV ozone treated substrate, with following input parameters to the spin coater.

Table 3.2: Parameters for CL deposition

Volume of solution (µl)	100
Rotating speed (rpm)	3000
Acceleration (rpm/sec)	500
Total time (sec)	30

Spin coated substrates were first set at 100 °C on the hot plate for drying afterward set at 500 °C for 40 minutes to calcinate in ambient to remove organic molecules from surface. At the end of annealing, when the temperature falls to room temperature they carried for next process.

2. **Electron transporting layer (ETL) preparation:**

Here, mesoporous TiO_2 is chosen as electron transport layer because of its good electron affinity and better matching of the bandgap with perovskite bandgap. Anatase TiO_2 has bandgap of 3.2 eV and electron affinity is 4.25 eV.

It was prepared by overnight stirring of TiO_2 paste with absolute ethanol, where the fraction of TiO_2:ethanol is 1:5.5. Here, 500 mg of TiO_2 paste mixed with 2750 mg of absolute ethanol.

- **ETL deposition:**

After synthesis of mp-TiO_2 it was spin-coated on UV-ozone treated CL with following spin-coater parameters.

Table 3.3: Parameters for ETL deposition

Volume of solution (µl)	100
Rotating speed (rpm)	5000
Acceleration (rpm/sec)	2500
Total time (sec)	25

Spin coated substrates were first set at 100 °C on the hot plate for drying afterward set at 500 °C for 40 minutes to calcinate in ambient to remove organic molecules from surface. After annealing, when the temperature falls to room temperature they kept 15 minutes for UV-ozone to increase surface energy before the perovskite layer deposition. Later, they transferred in to the glove box for the next step.

3. **Perovskite active layer preparation:**

It was prepared in glove box to reduce the exposure to humidity and oxygen. Total 600 µl $MAPbI_3$ was prepared with 1.4 M concentration. 133.476 mg of MAI and 387.24 mg of PbI_2 were mixed followed by addition of 600 µl DMF. The whole solution was kept for overnight stirring at room temperature.

- **Perovskite layer deposition:**

This has to be done in glove box due to environmental instability of $MAPbI_3$. Anti-solvent has to be dripped before nine seconds of completion of spin-coating.

Table 3.4: Parameters for perovskite deposition

Volume of Perovskite solution (µl)	50
Volume of dripping solvent (µl)	100
Rotating speed (rpm)	5000
Acceleration (rpm/sec)	2500
Total time (sec)	13

4. Hole transporting layer (HTL) preparation:

Spiro-OMeTAD is used as HTL here. It was prepared by 70 mg of spiro-OMeTAD dissolved with the help of 1 ml of chlorobenzene followed by incorporation of tert-butylpyridine with 28 µl and lithium bis(trifluoromethylsulfonyl)imide (50 mg of Li-TFSI in 100 µl acetonitrile) with 20 µl directly. Already dissolved Co-dopant tris(2-(1H-pyrazol-1-yl)-pyridine)cobalt(iii) tris(trifluoromethylsulfonyl)imide (FK 102 Co(iii) TFSI salt, Dyesol) in acetonitrile which was also included to the HTM solution.

- **HTL deposition:**

Hole transporting material spiro-OMeTAD solution was deposited after perovskite layer cools down to room temperature, with following spin-coating parameters.

Table 3.5: Parameters for HTL deposition

Volume of solution (µl)	50
Rotating speed (rpm)	5000
Acceleration (rpm/sec)	2500
Total time (sec)	25

5. Electrode deposition:

Finally, with the help of thermal evaporator gold electrode of nearly 100 nm thickness was deposited using 0.2 cm^2 mask.

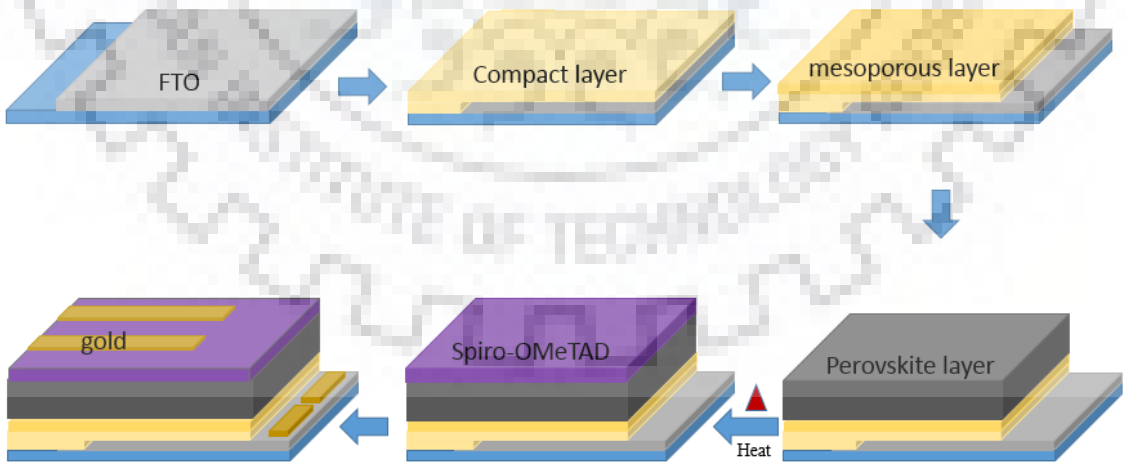

Figure 3.3: Device fabrication steps

CHAPTER 4: Characterizations of films

Characterization is carried out with the help of instruments listed in the **table (4.1)**.

Table 4.1: Instruments used for characterization

characterization	***Instrument***	***Remark***
Optical absorption	UV-3600 UV-vis-NIR spectrophotometer (shimadzu)	350 nm to 850 nm
Photoluminescence	Acton Spectra Pro 2500i spectrometer and Princeton Instruments PIXIS 400 CCD camera	650 nm to 850 nm
X-ray diffraction	Bruker AXS D8 ADVANCE and Panalytical	Cu Kα λ = 1.5418 Å
Scanning electron microscopy	FESEM JEOL JSM-7600F	
J-V characteristics	Solar simulator (Newport 91190A) with xenon lamp of 450 W	0.09cm^2 Mask used
Atomic force microscopy	Asylum research MFP-3D	Silicon tip
Fourier-transform infrared spectroscopy	FluoroMax-4	With ATR

4.1: UV-visible spectroscopy

This spectroscopy technique is widely used in solar cell film characterisation. The photons are incident on the thin film, powder or solution and absorbance is measured. It uses the photons with energy lies in ultraviolet to visible region. The semiconductor material will absorb the photons with energy minimum to its bandgap and higher than that, while photons with energy less than its bandgap will get transmitted. From this characterisation bandgap can be measured by plotting tauc plot.

First trial of spin coating of $MAPbI_3$ was done on the glass substrate to measure its optical properties. Two samples were prepared with 70 µl of $MAPbI_3$ solution and 150 µl of anti-solvent dripped after 5 second of spinning started, where one dripping was fast and other one was slow.

As it was first time spin coating in glovebox due to lake of skills it is showing some different behavior when compared with each other. Here, UV-vis spectroscopy shows that the region between 770 nm to 800 nm is same for both, while below 770 nm the absorbance of the sample 1 raises higher compared to sample 2, which indicated that the thickness of the sample is quite more or due to difference in the dripping process.

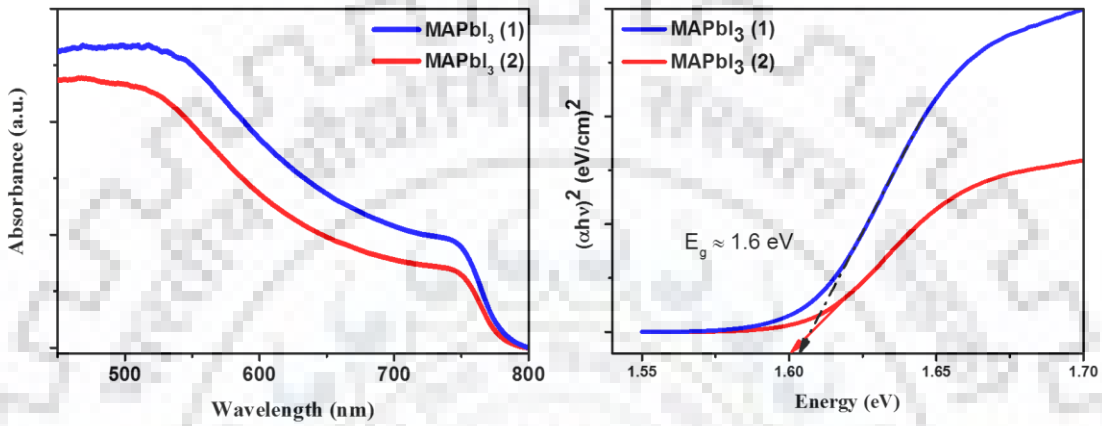

Figure 4.1: (a) Optical absorption (b) Tauc plot (of trial films)

Both samples have quite same band gap of around 1.6 eV which is calculated from tauc plot as shown in the graph in the small window, it confirms with the theoretical understanding that the

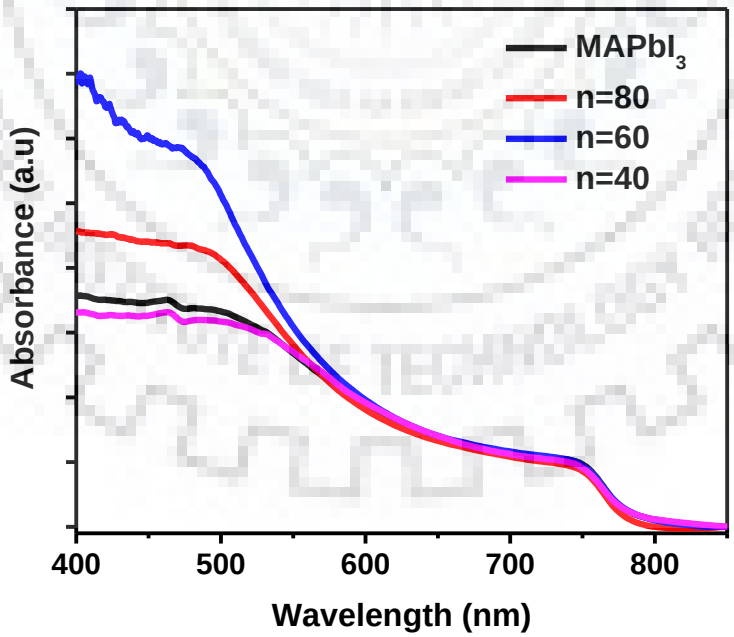

Figure 4.2: Optical absorption comparison of $MAPbI_3$ and $(R)_2(MA)_{n-1}Pb_nX_{3n+1}$

material and processing condition are the same than the bandgap should be the same but there will be differences due to difference in the dripping process which leads to difference in crystallization and growth.

When the optical properties of the $MAPbI_3$ and $(R)_2(MA)_{n-1}Pb_nX_{3n+1}$ compared through SHIMADZU UV-VIS-NIR spectrophotometer UV 3600 plus it exhibit quite similar optical absorption as shown in figure 4.2. However, n with 60 shows a notably stronger absorbance below 600 nm, while n with 80 is showing second highest absorbance followed by pure $MAPbI_3$ and lowest absorbance is exhibited by n = 40 when compared below 550 nm. The absorbance profile of all the films are showing absorbance band edge around 800 nm. It has been observed that bit shift in the absorption edge of the films at 770 -780 nm.

4.2: FTIR

This spectroscopy method is uses IR region of radiation. IR radiation is incident on material, material will absorb the frequency which corresponds to functional chemical groups such as methyl ($-CH_3$), hydroxyl (-OH), imido (NH), and amido ($-NH_2$) attached. These groups absorbs

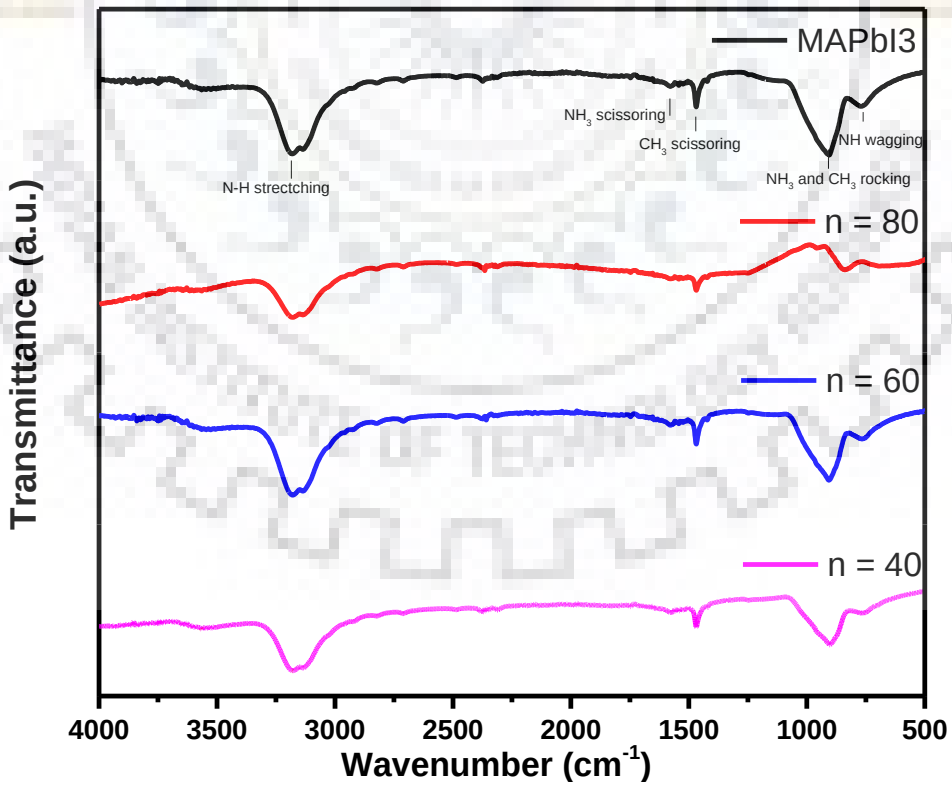

Figure 4.3: FTIR comparision for $MAPbI_3$ and $(R)_2(MA)_{n-1}Pb_nX_{3n+1}$

IR photons at a characteristic frequency but actually it may differ depending upon the environment. In organic perovskite amido (-NH_2) group is present, so as to confirm the formation of perovskite in thin film and to find out any adsorbed species on the surface, FTIR measurement has to be carried out.

$MAPbI_3$ has CH_3NH_3 which exhibits absorbance of IR waves in FTIR. Here, as shown in the figure 4.3 NH stretching, NH_3 scissoring, CH scissoring, NH_3 and CH_3 rocking, and NH wagging are observed at 3181.97 cm^{-1}, 1582.3 cm^{-1}, 14852 cm^{-1}, 907.34 cm^{-1}, and 769.45 cm^{-1} respectively.

FTIR spectroscopy is used to confirm the presence of PEA^+ and SCN in the prepared $(R)_2(MA)_{n-1}Pb_nX_{3n+1}$ films. The presence of C = C bond stretching around at 1600 cm^{-1} due to existence of benzene ring of the PEA, while existence of the C ≡ N of SCN should be observed between 2000 to 2100 cm^{-1}.

FTIR used is FluoroMax-4 with Attenuated total reflectance (ATR) sampling technique. Here, in the spectrum no such sign is visible, this may be because of very less amount of PEA(SCN) that has been added to from LD. This ATR-FTIR is scans at very small area of total film area, so it is hard to detect the presence of the very small amount of additive.

4.3: XRD

In this characterization X-rays are incident on the sample. As the X-rays has high energy it will penetrate into the sample up to certain depth and gets diffracted due to atom and their arrangement. Diffracted x-rays contains the information of the crystal structure, crystallite size and different phases present in the sample. Perovskite material shows temperature dependent crystal structure, so it is necessary to get the crystal structure information of the perovskite absorbing layer.

X-ray diffraction measurements were carried out on Panalytical XRD and peak matching analysis is carried using MATCH software. $MAPbI_3$ is showing peaks nearly at 14.12º, 20º, 23.5º, 24.5º, 28.45º , 31.9º, 34.9º, 38.7º, 40.6º, 42.6º, 43.2º and 52.5º from which major intense peaks are assigned to planes (110), (220) and (310) for 2θ values 14.12º, 28.45º and 31.9º respectively. The peak at 12.69º is attributed to residual PbI_2 that present in the film, while peak at the 38.62º shows combined effect of the PbI_2 and $Pb(SCN)_2$.

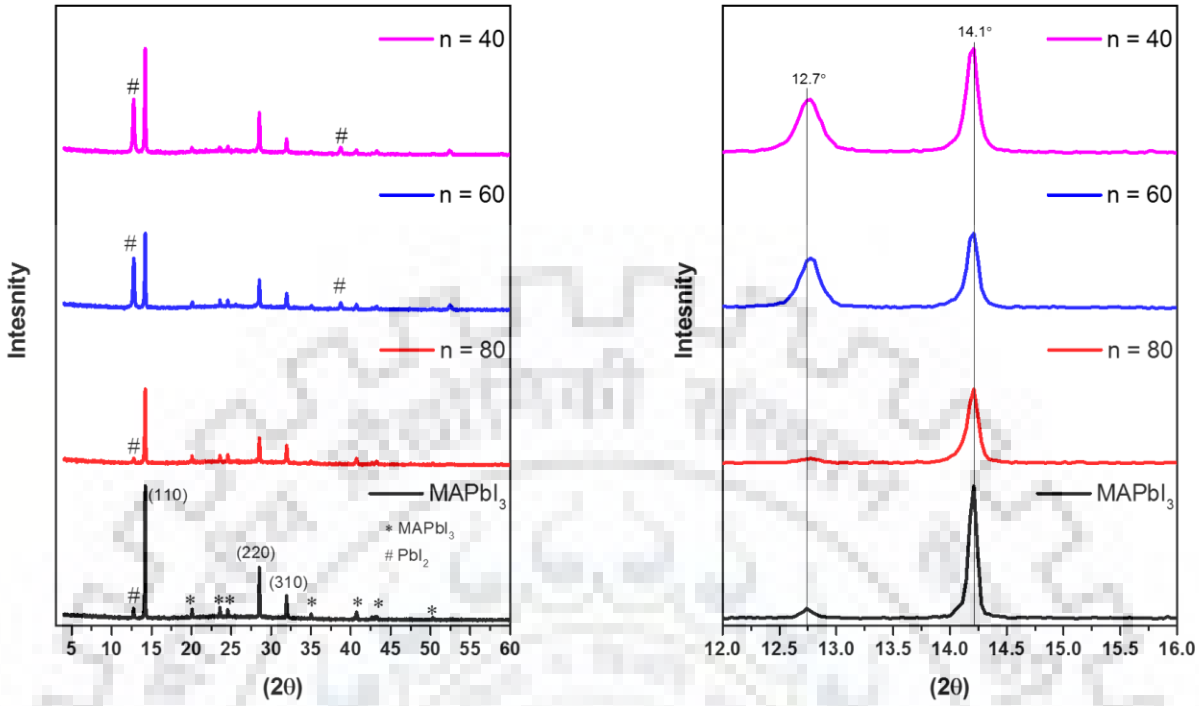

Figure 4.4: (a) X-ray diffraction patterns (b) Magnified patterns for $MAPbI_3$ and $(R)_2(MA)_{n-1}Pb_nX_{3n+1}$

As shown in the figure 4.4, $(R)_2(MA)_{n-1}Pb_nX_{3n+1}$ with n=80 is showing very small peak compared to others which is indication of the very less amount of residual PbI_2 present which can makes it good as an active layer. In addition, ratio of intensity of the first perovskite peak and the lead iodide peak is higher. Nan Li et al. has reported that, as we move from 3D perovskite to reduced dimensional perovskite with PEA cation, the full width half maximum (FWHM) lowers down because improved crystallinity [64]. Here, as the dimensionality is reduced FWHM is increases which suggest that the crystallinity is adversely affected, which can be attributed to thiocyanate anion. It confirms that quasi-2D formation not taking place due to missing low angle peaks.

4.4: AFM

Atomic Force Microscopy is technique which uses the nano-sized cantilever to measure the surface properties like roughness, adhesion, phases present on the surface etc.

Performance of the solar cell is highly dependent on the roughness of the layers. So it makes important to measure quantitatively the surface roughness of the film. Apart from roughness, AFM

is capable to measure lot many other quantities like surface potential, work function of material and IV characteristic.

AFM of the first attempt of $MAPbI_3$ film is carried out using Asylum Research MFP-3D model of AFM. The figure shows scanned image of scan area of 90 μm^2 where particles of $MAPbI_3$ are clearly visible. The particles are larger in size during play with dripping process.

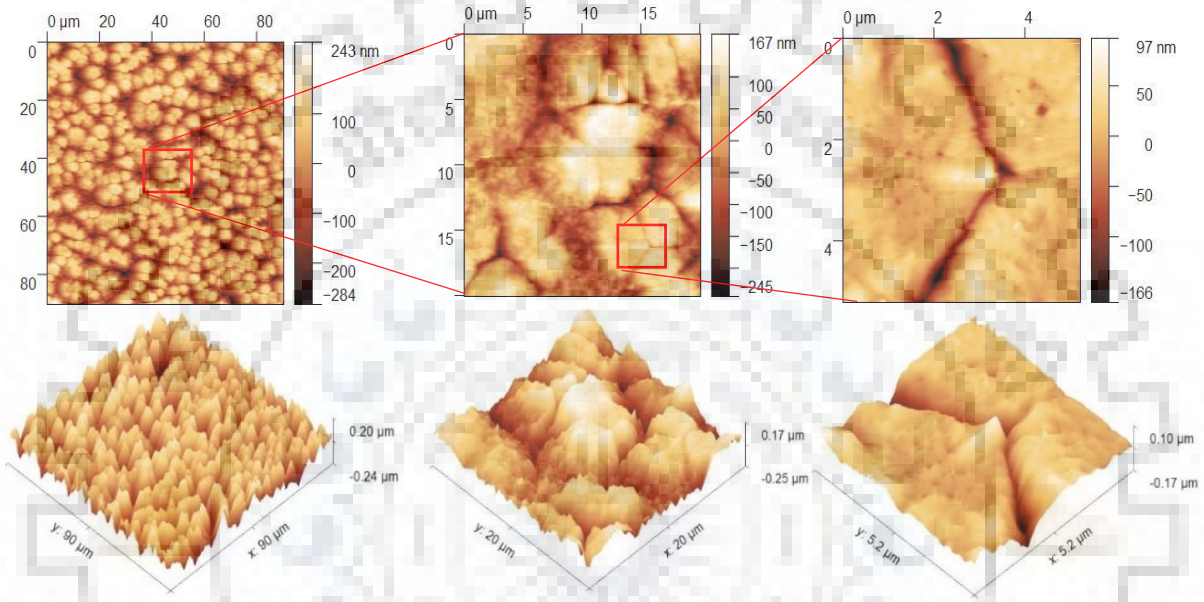

Figure 4.5: AFM image of trial pure $MAPbI_3$ film
[2D (top) and 3D (bottom) with magnified scanned images (from left to righ)]

4.5: SEM

Scanning Electron Microscopy is important tool of surface measurement. It uses the focused electron beam to scan surface of the sample and detector will collect secondary electrons emitted from surface of the sample. It will give the information regarding the morphology i.e. shape, size of the sample. It can be used to get the cross-sectional image of the sample from which thickness of the different layers can be calculated.

JOEL JSM-7600F Scanning Electron Microscope is used to get the morphological information of the prepared films. Image of $MAPbI_3$ states that the grains are randomly oriented with grain size approximately 400 nm to 500 nm and broader grain size distribution. So, the pure $MAPbI_3$ has overall rough morphology. Addition of very small amount of PEA(SCN) i.e. n = 80 is exhibiting

smooth morphology with compact grains and without pinholes. Apart from that, it is showing the smaller grains of 100 nm. As the amount of PEA(SCN) is increased it is showing two different morphology. Two phase mixture as compact grain and small grains are visible in n = 60. The

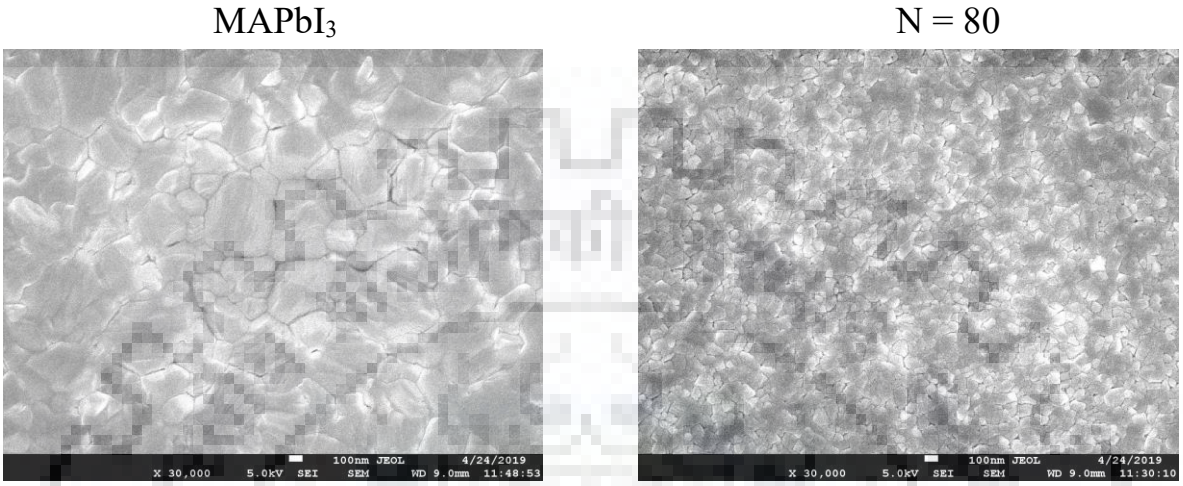

Figure 4.6: Top SEM image for $MAPbI_3$ and $(R)_2(MA)_{n-1}Pb_nX_{3n+1}$

morphology with lot of pinholes and increased roughness was obtained when amount of PEA(SCN) added i.e. n = 40 which is also confirmed with the AFM scan.

CHAPTER 5: Results and discussion

5.1: Moisture stability study:

To investigate the moisture stability of the prepared perovskite materials, their films were kept in ambient environment with around 50% RH and room temperature for three days and followed by different characterisations as follows.

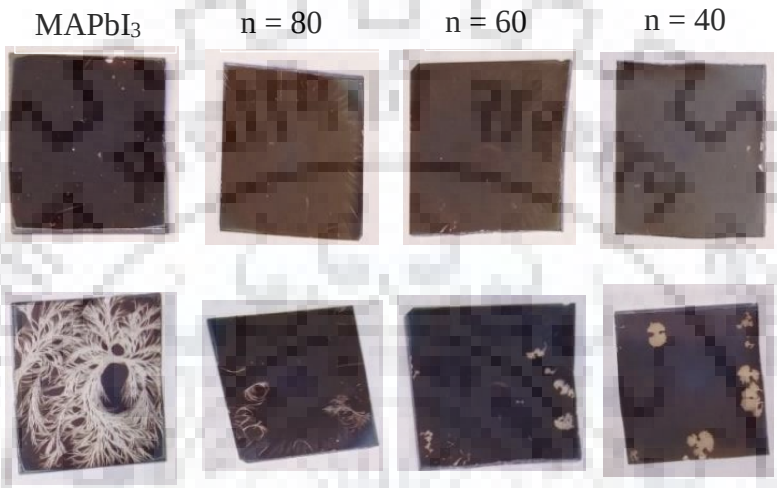

Figure 5.1: Images of prepared films before (top) and after moisture study (bottom) For $MAPbI_3$ and $(R)_2(MA)_{n-1}Pb_nX_{3n+1}$

5.1.1: UV–visible spectroscopy

Here, absorption spectra show that after incorporation of the hydrophobic cation (PEA^+). It provides protection from the moisture. As it is clearly visible that the pure $MAPbI_3$ is loses its absorption after three days in ambient. Whereas the $(R)_2(MA)_{n-1}Pb_nX_{3n+1}$ with lowest n value (n = 40) is still retaining its absorption. So, as the concentration of the ligand increases its moisture stability increases.

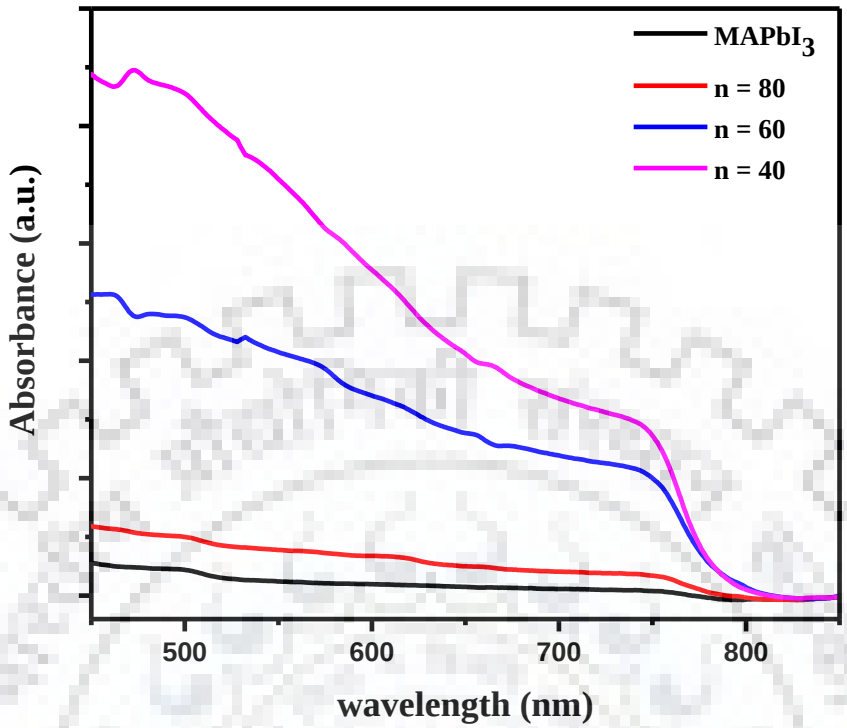

Figure 5.2: Optical absorption after 3 days exposure to moisture For $MAPbI_3$ and $(R)_2(MA)_{n-1}Pb_nX_{3n+1}$

5.1.2: AFM

Here, an attempt is made to study the effects after moisture exposure on grains using the AFM.

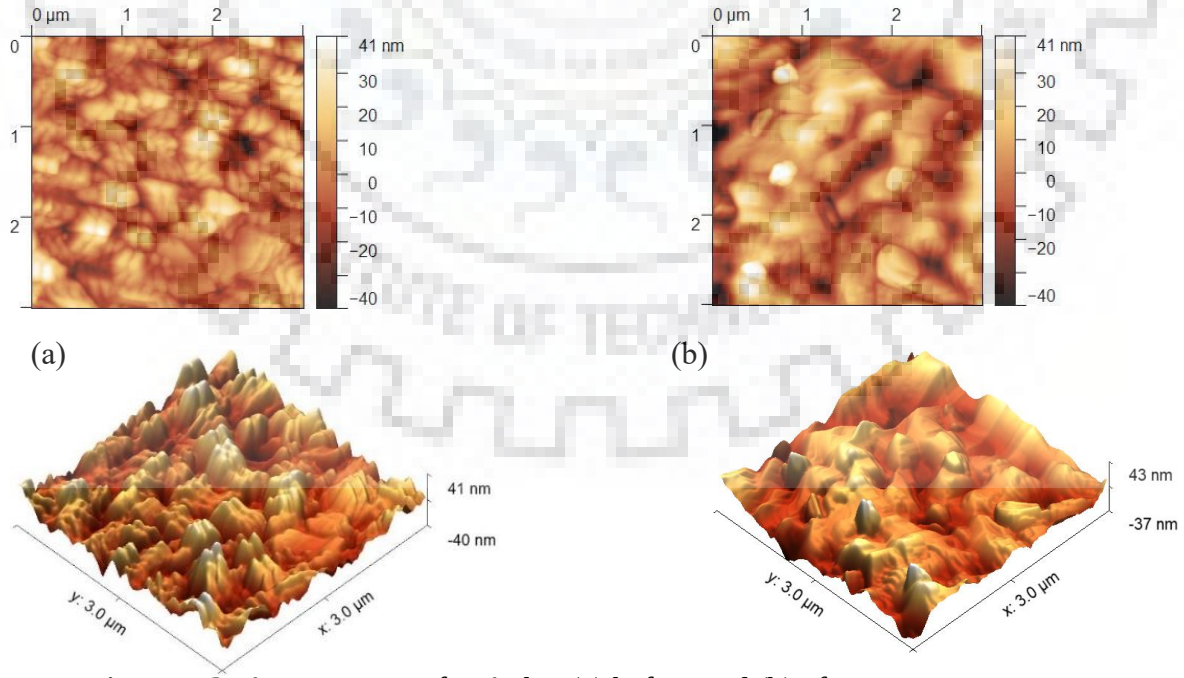

Figure 5.3: AFM images of $MAPbI_3$ (a) before and (b) after moisture exposure

Before moisture test, $MAPbI_3$ film was showing the root mean square roughness of 11.19 nm, while 15.37 nm, 21.44 nm, 30.76 nm for n value of 80, 60, 40 respectively for the scanned area of 100 μm^2. Addition of the PEA and thiocynate results in the smaller grains and increased roughness, which is supported by the AFM images. Preferred orientation is seen in which maximum PEA(SCN) is added.

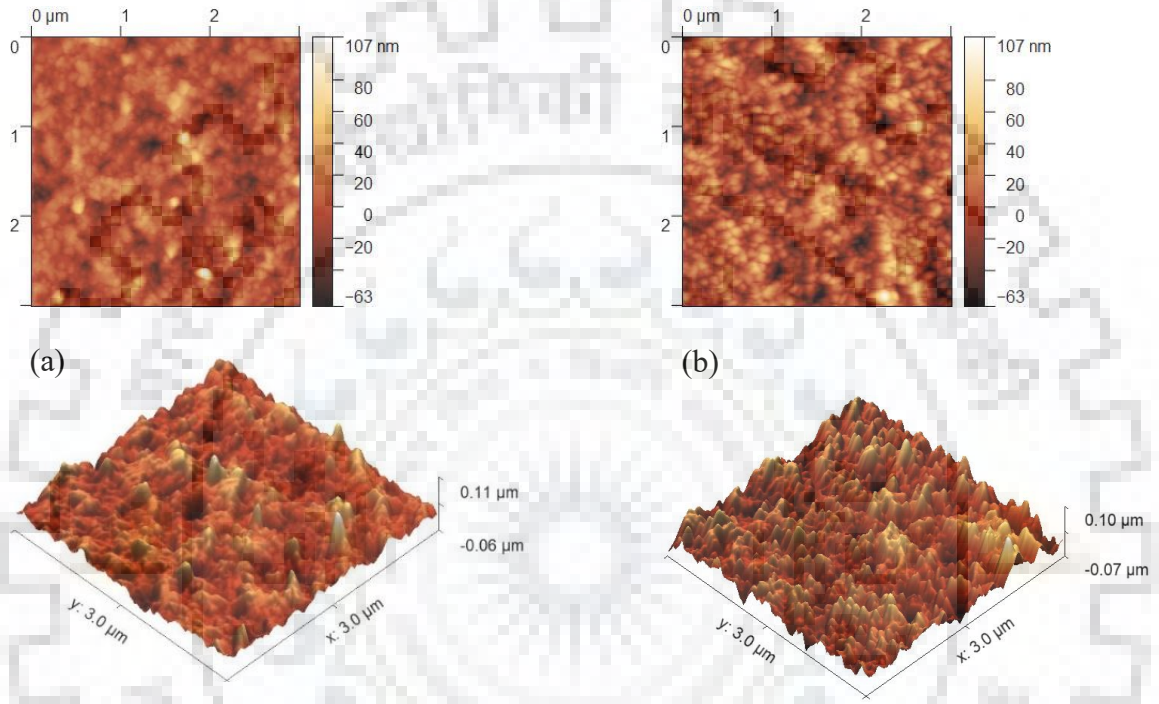

Figure 5.4: AFM images of $(R)_2(MA)_{n-1}Pb_nX_{3n+1}$ for n=80 (a) before and (b) after moisture exposure

For pure $MAPbI_3$ film after exposure to moisture, it is clearly visible that moisture destroys the grains. Inter diffusion of grains in the presence of the moisture which is most likely due to ionic diffusivity of an organic salt. Water cannot penetrate easily in to system due to ammonium ligand. For n = 40, it seems that the water inclusion from the pinholes creating space between group of grains i.e. bulging is taking place. Moisture affected the surface roughness, the roughness value for $MAPbI_3$, n = 80 and n = 60 are around 194 nm, 16.146 nm, and 23.208 nm respectively. Whereas for n = 40 initial film was more rough because of its grain growth and after moisture

penetration in the pinholes its roughness decreases to 26.510 nm. All the roughness values are for scanned area of 100 μm^2.

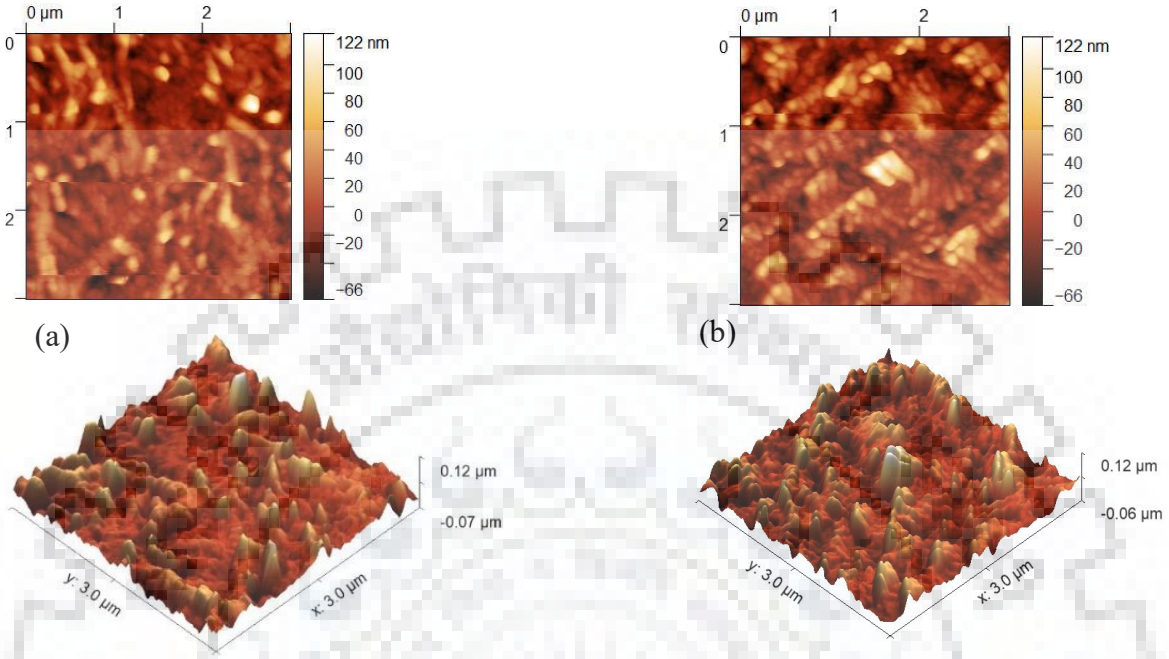

Figure 5.6: AFM images of $(R)_2(MA)_{n-1}Pb_nX_{3n+1}$ for n=60 (a) before and (b) after moisture exposure

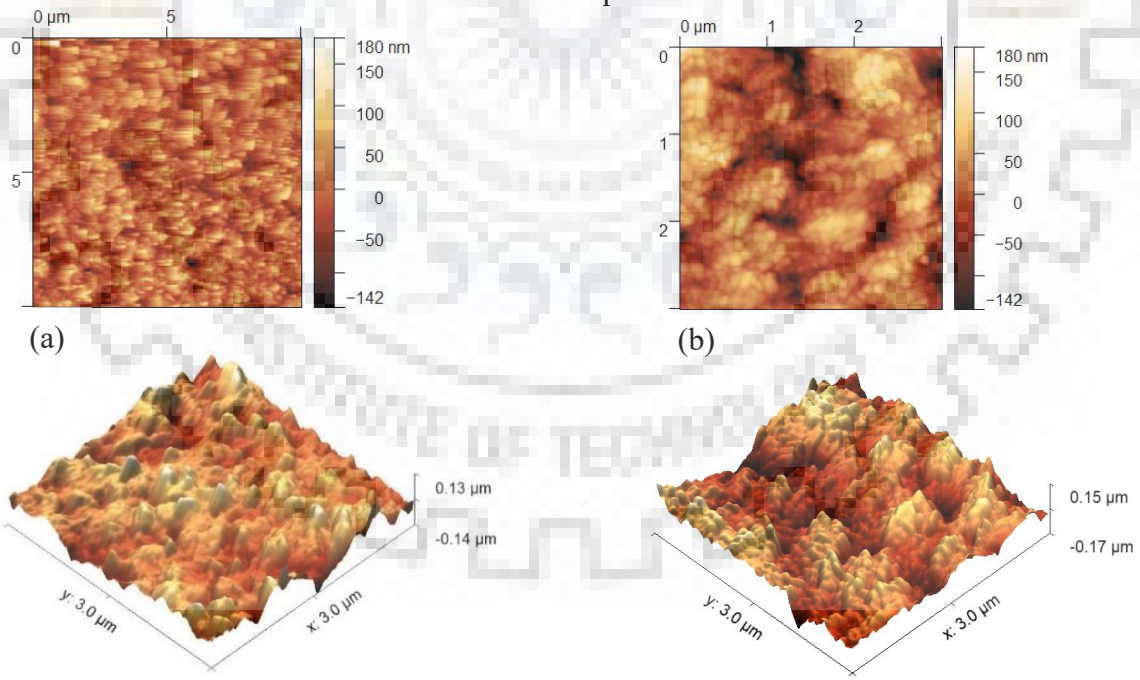

Figure 5.5: AFM images of $(R)_2(MA)_{n-1}Pb_nX_{3n+1}$ for n=40 (a) before and (b) after moisture exposure

5.1.3: Water contact angle

Water contact angle measurement helps to determine the surface characteristics towards the water. If the surface is hydrophobic then it will give the contact angle more than 90° while the hydrophilic surface will give less than 90°.

Here, this measurement is carried out to study the effect of addition of PEA(SCN) on the surface. Perovskite is ionic compound, so it is hydrophilic in the nature which can be seen from the figure 5.7 that it is giving the average contact angle of 86.4°. Due to its hydrophilicity this measurement

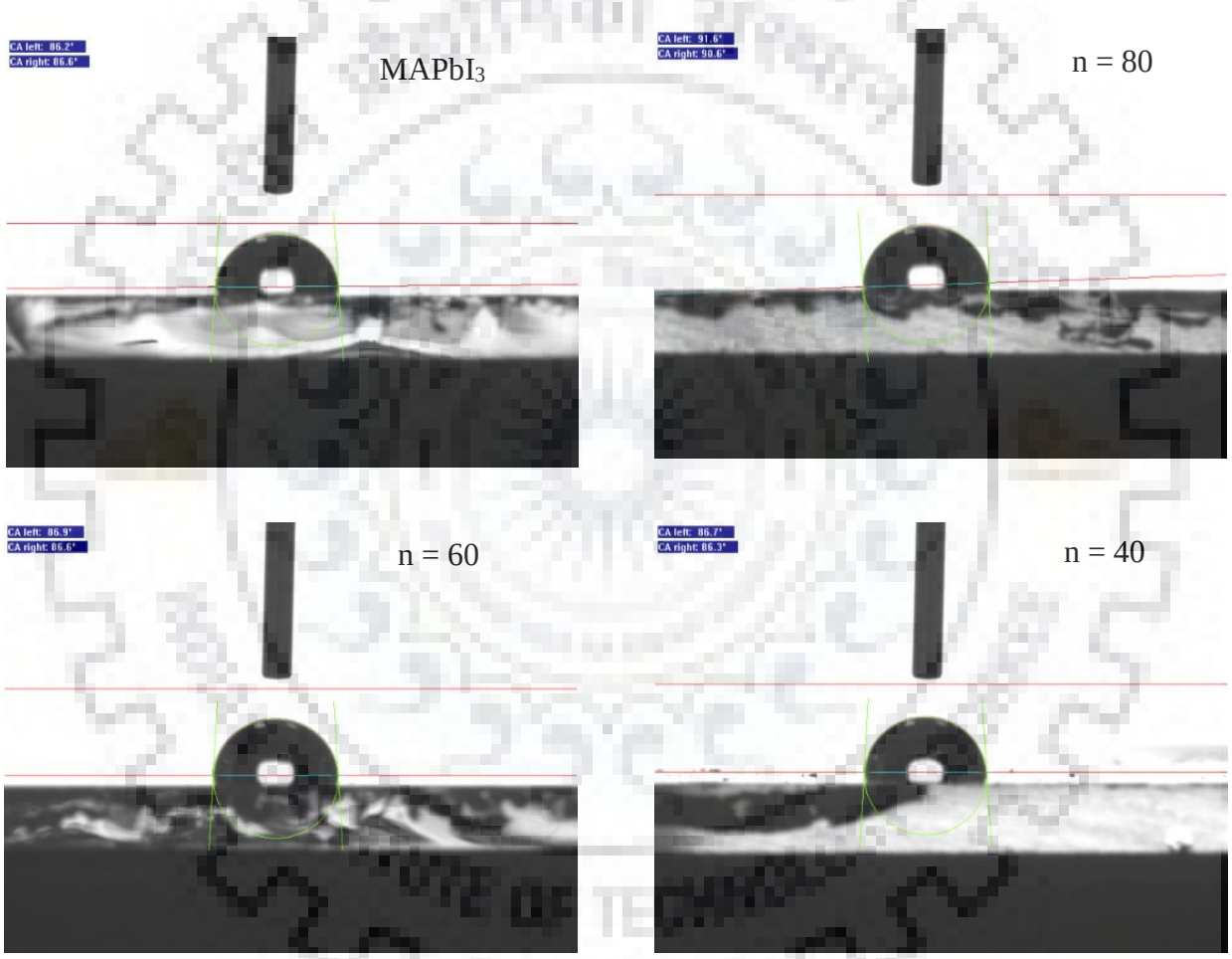

Figure 5.7: Surface hydrophobicity test for $MAPbI_3$ and $(R)_2(MA)_{n-1}Pb_nX_{3n+1}$

has done with respect to time, in that regards it has shown the drastic decrement up to 60.8° within four seconds and started showing the yellow colour PbI_2. $(R)_2(MA)_{n-1}Pb_nX_{3n+1}$ with 80, 60, 40 n values are showing average contact angle of 91.1°, 86.75° and 86.5° respectively.

As the amount of PEA(SCN) increases the average contact angle first increases than decreases. This unexpected behaviour is may be due to more pinholes on the surface when added ligand is higher than certain molar ratio the as described in SEM images. Interestingly, the higher molar ratio of PEA(SCN) doesn't allow the water molecule to spread, so with time the decrement in the average contact angle is very less compared to pure $MAPbI_3$. So, the highest contact angle in n = 80 film is because of the grain size is very small and compact morphology as depicted in the SEM image and AFM image. So up to certain quantity PEA(SCN) is helping to improve the surface hydrophobicity.

5.2: Study of devices:

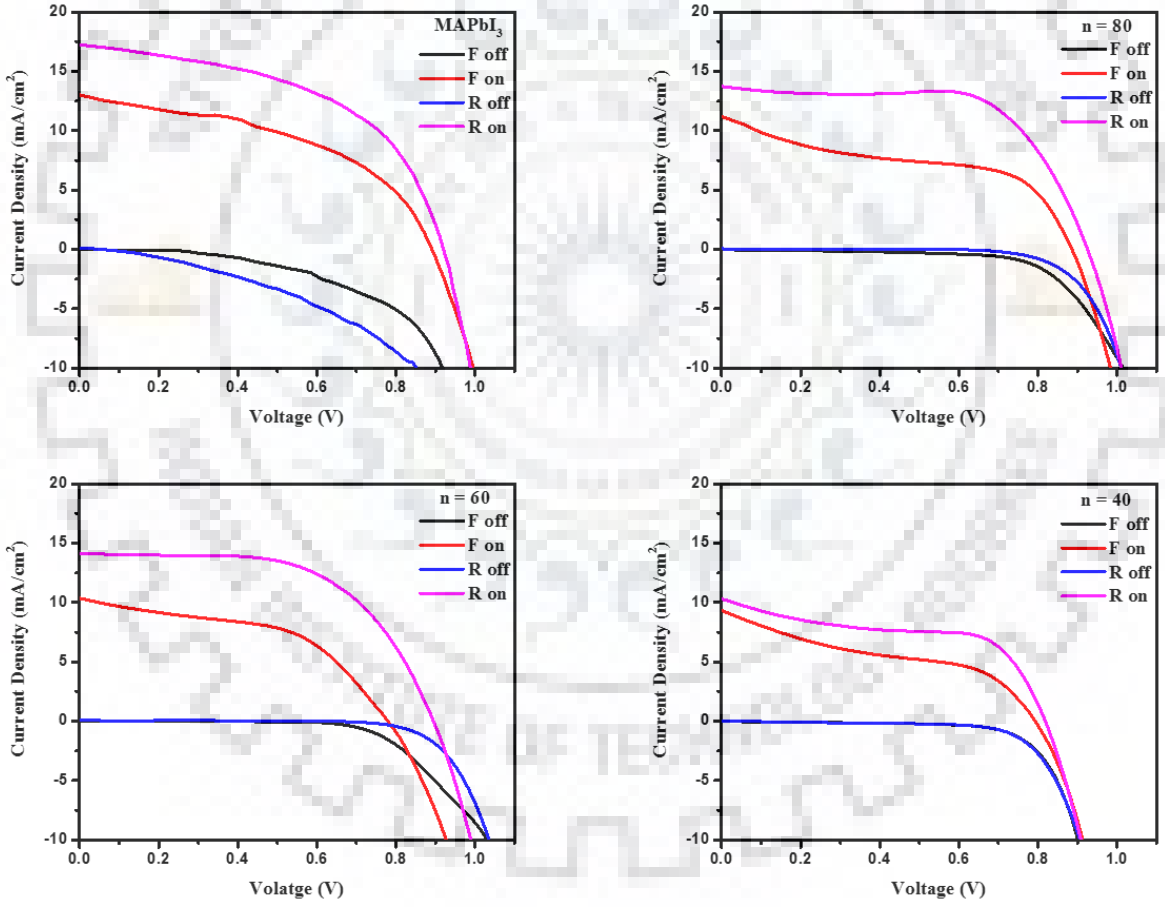

Figure 5.8: J-V performance of devices of $MAPbI_3$ and $(R)_2(MA)_{n-1}Pb_nX_{3n+1}$ with n=80, n=60, n=40 (F: forward, R: reverse, off: dark, on: light)

The performance of the PSCs utilizing conventional device architecture is depicted in Fig. The J-V characteristics of devices were measured with solar simulator under AM1.5G illumination at

100 mW/cm^2. Pervoskite solar cells fabricated with pure $MAPbI_3$ depicts PCE of 8.81% with a fill factor of 54.42%, current density of 17.40 mA/cm^2, and open circuit voltage of 0.93 V (**Table (5.1)** , **Figure (5.8)**). The PCE of the device with smaller doping of PEA(SCN) (n = 80) reduces slightly (8.31%) mainly due to reduction in the current density from 17.40 to 13.74 mA/cm^2 in compare to pure $MAPbI_3$. However, these devices observe significant enhancement in the fill factor from 54.42% to 65.46% to pure $MAPbI_3$. Further addition of the PEA(SCN) has an adverse affect on the performance of solar cell owing to reduction in the current density by passivation the pervosktie nanocrystals. However, fill factors slightly decreases to 59.01% (n = 60), and 56.14% (n = 40) than n = 80 but still higher than that of pure $MAPbI_3$. Moreover, as discussed earlier that the moisture stability improves significantly with an addition of a long ammonium ligand. Although PCE with small amount of doping of PEA(SCN) somehow remains the same but moisture stability of the devices has been taken care for by mixed 3D-2D mixture.

Table 5.1: Performance paratmeters for highest efficiency devices

$(R)_2(MA)_{n-1}Pb_nX_{3n+1}$	Voc (V)	J_{sc} (mA/cm^{-2})	Fill Factor (%)	Efficiency (%)
Pure $MAPbI_3$	0.93	17.40	54.42	8.81
n = 80	0.92	13.74	65.46	8.32
n = 60	0.89	14.14	59.01	7.46
n = 40	0.81	10.31	56.14	4.73

The n = 40 is showing the lowest hysteresis followed by n = 80, pure $MAPbI_3$ and at last n = 60. There is systematic decrease in the V_{oc} from n = 80 to n = 40, which suggest that grain boundary passivation by organic cation takes place in n = 80 but some ambiguous effect takes place in high concentration additive perovskite.

The J_{sc} is decreasing gradually from 17.4 mA/cm^2 to 10.31 mA/cm^2 for $MAPbI_3$ to n = 40 respectively. Mixed dimensional perovskite exhibits lower current density due to hassle to effective charge transport mechanism.

Addition of PEA(SCN) is improving the fill factor, as the highest fill factor observed is 65.46% for n = 80 device. Whereas, fill factor is showing decrement as the content of PEA(SCN) increases

but still that is higher than the pure $MAPbI_3$. The additive is also showing the effect on the hysteresis behaviour, which can be able to reduce the hysteresis.

5.2.1: Performance after first attempt of optimization

In the first trial of the devices fabrication efficiency of the devices were low because of less skill and experience. So, first trial of optimization is carried out which resulted in the efficiency of 14.8% for the pure $MAPbI_3$ but still less efficiency for the other devices.

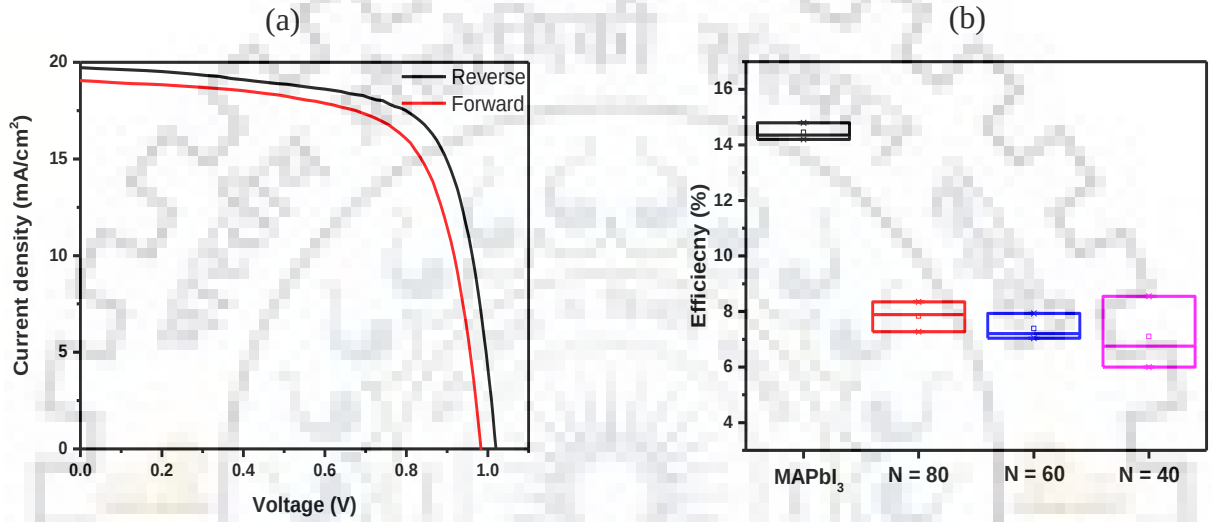

Figure 5.9: (a) Highest J-V performance of device of $MAPbI_3$ (b) statistical data for the various devices efficiency after first optimization for $MAPbI_3$ and $(R)_2(MA)_{n-1}Pb_nX_{3n+1}$

Table 5.2: Performance paratmeters for highest efficiency devices after first optimization

	V_{oc} (V)	J_{SC} (mA/cm^2)	Efficiency (%)	FF (%)
$MAPbI_3$	1.01	19.72	14.80	71.39
N = 80	0.86	15.58	8.35	61.71
N = 60	0.86	14.85	7.93	61.83
N = 40	0.90	15.19	8.55	62.21

After first trial of optimization, cross-sectional SEM (scale of 100 nm) is carried out to see the interfaces and thickness of different layers. The thickness of perovskite layer, mesoporous layer and hole transporting layer is approximately 350 nm, 250 nm and 200 nm respectively. Reference cell got highest efficiency of 14.8%, still it need further optimization because poor contact has been observed from its cross-sectional image. All the images are showing the poor contact at the mesoporous and compact layer interface which is inducing the resistance due to which efficiency is less, which indicates the possibility of further enhancement of the efficiency for the devices. From top the fisrt layer is of gold, second layer is of sipro-OMeTAD which has many pinholes which is not good for performance. Third layer from top is perovskite layer whie fourth layer mesoporous layer of TiO_2. Compact layer of TiO_2 is very thin in between meso layer and FTO. Elongated grains are visible for the n = 40 which may be due to decrease in the dimensionality but still it is not confirmed with XRD.

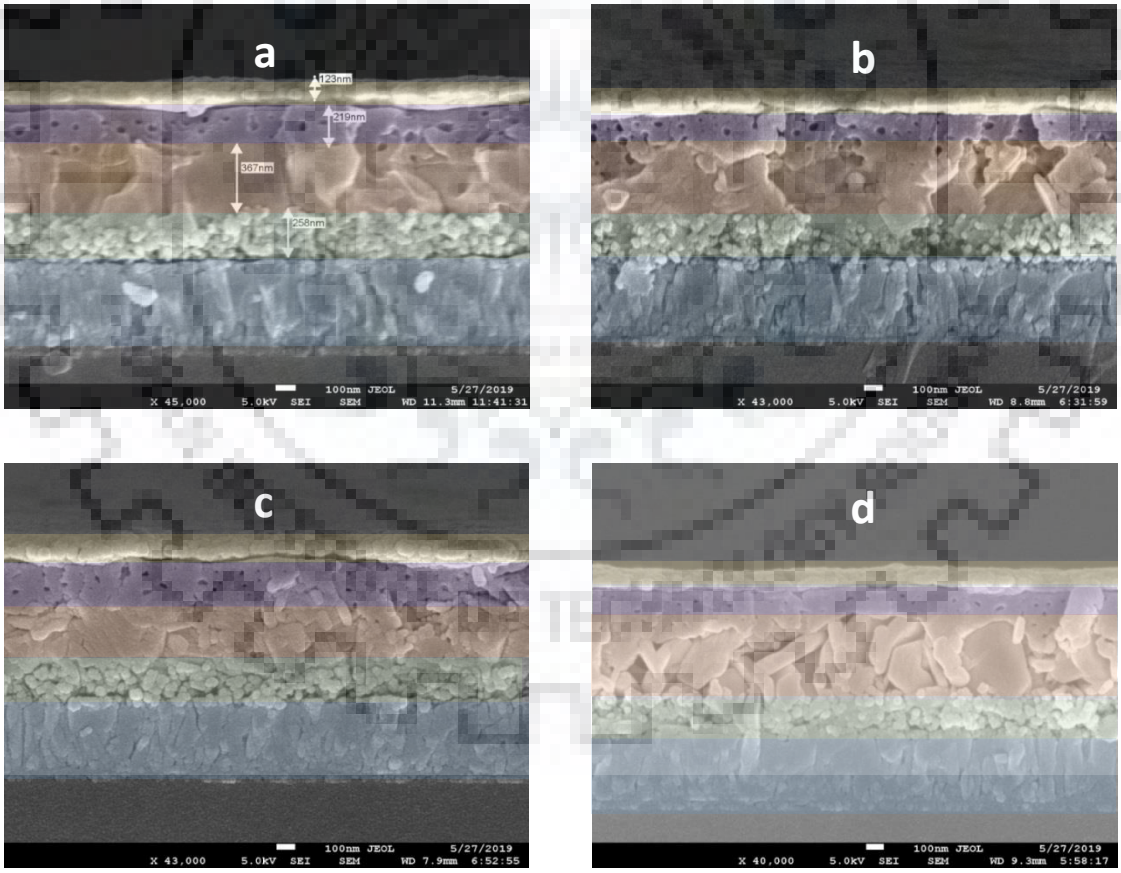

Figure 5.10: Cross-sectionali SEM of devices for (a) $MAPbI_3$ and (b), (c), (d) with n = 80, n = 60 and n = 40 in $(R)_2(MA)_{n-1}Pb_nX_{3n+1}$

5.2.2: Device stability study:

To study the variation in the efficiency of the devices in the ambient condition they were kept in drybox with relative humidity 50% at room temperature. After 24 hrs their efficiency is calculated for two days.

It has been observed that the drop in the efficiency for the less amount of PEA(SCN) is very less compared to other although its efficiency is not that comparable to the reference cell but it can be further improvised. While addition of more PEA(SCN) is showing poor stability and as compared to the pure $MAPbI_3$. In the first 24 hrs device of n = 80 is showing quite good stability compared to successive 24 hrs. To increase the stability further encapsulation can be adopted.

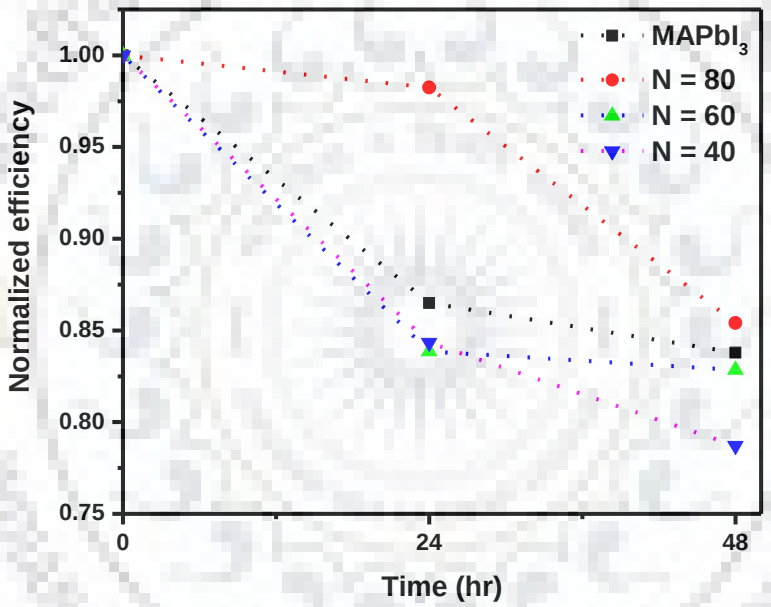

Figure 5.11: Device stability with time

The ligand is forming the mixed 3D/2D structure or giving the passivation effect is still a question, as both the signatures have been observed in various measurement. Still a strong evidence is required to understand the interaction of this organic ligand with the perovskite. As this experimentation is performed by less skills, further chances of enhancement in the results are possible.

CHAPTER 6: Conclusions and future scope

In conclusion, addition of phenylethylammonium thiocyanate PEA(SCN) in a certain molar ratio can enhanced the moisture stability without losing much of the device performance. The highest efficiency achieved is 14.8% for $MAPbI_3$ while n = 80 exhibited efficiency of 8.3% with improved stability in the efficiency. It has been also observed that $(R)_2(MA)_{n-1}Pb_nX_{3n+1}$ with n = 80 exhibits compact morphology while the more amount of phenylethylammonium thiocyanate is resulting in the worse morphology. Using atomic force microscopy it has been concluded that the roughness of the $MAPbI_3$ is higher compared to $(R)_2(MA)_{n-1}Pb_nX_{3n+1}$ after moisture exposure. Whereas the n = 40 exhibited reverse phenomenon of decreasing the roughness of the film after exposure to moisture for three days due to its pinhole and prior rough morphology. Interestingly, surface hydrophobicity examined from the water contact angle demonstrated that the less content of phenylethylammonium thiocyanate that is n = 80, is giving the hydrophobic surface with contact angle of more than 90º. That may be sign of surface passivation by organic cation of the phenylethylammonium thiocyanate. None of them has exhibited quasi-2D characteristics. Results obtained are preliminary and further optimizations are required.

As discussed, the main challenges for any solar cell technology is efficiency, cost and stability, among those perovskites has shown extraordinary success in the growth of efficiency and lowering the cost of fabrication. While stability is not that explored as compared to efficiency. So stability is a major concern for perovskite materials as they are ionic materials. Stability issue can be handled via intrinsic improvement of properties using ambient stable additives or dopping, which can enhance the crystallinity, hydrophobicity and thermal resistance. Using hybrid dimensional mixed perovskite is one of the better way to improve the ambient stability without loosing much of the performance. Incorporating inorganic components in the hybride dimensional mixed perovskite may further enhance the ambient stability as they are more stable as compared to organic counterpart. The grain boundaries are more susceptible to degradation, to overcome that passivation with organic molecules should be adopted. Using positive sides of all the approaches one can improve performanace with enough stability.

Remarkably, perovskite material has huge potential for attaining durable solar cells and still expects further exploration.

References

1. Im, J.-H., et al., *6.5% efficient perovskite quantum-dot-sensitized solar cell.* Nanoscale, 2011. **3**(10): p. 4088-4093.
2. Jena, A.K., A. Kulkarni, and T. Miyasaka, *Halide Perovskite Photovoltaics: Background, Status, and Future Prospects.* Chemical Reviews, 2019. **119**(5): p. 3036-3103.
3. Kojima, A., et al., *Organometal Halide Perovskites as Visible-Light Sensitizers for Photovoltaic Cells.* Journal of the American Chemical Society, 2009. **131**(17): p. 6050-6051.
4. Kim, H.-S., et al., *Lead Iodide Perovskite Sensitized All-Solid-State Submicron Thin Film Mesoscopic Solar Cell with Efficiency Exceeding 9%.* Scientific Reports, 2012. **2**: p. 591.
5. *World Energy Outlook 2017.* International Energy Agency, 2017.
6. Hegedus, P.A.L.a.D.S., *Handbook of Photovoltaic Science and Engineering.* John Wiley & Sons, Inc., 2010: p. 1164.
7. National Renewable Energy Laboratory (NREL).
8. Hans-Rudolf Wenk, A.B., *Minerals: Their Constitution and Origin*. 2004.
9. Goldschmidt, V.M., *Krystallbau und chemische Zusammensetzung.* Berichte der deutschen chemischen Gesellschaft (A and B Series), 1927. **60**(5): p. 1263-1296.
10. Li, C., et al., *Formability of ABX3 (X = F, Cl, Br, I) halide perovskites.* Acta Crystallographica Section B, 2008. **64**(6): p. 702-707.
11. Frost, J.M., et al., *Atomistic Origins of High-Performance in Hybrid Halide Perovskite Solar Cells.* Nano Letters, 2014. **14**(5): p. 2584-2590.
12. Lee, M.M., et al., *Efficient Hybrid Solar Cells Based on Meso-Superstructured Organometal Halide Perovskites.* Science, 2012. **338**(6107): p. 643-647.
13. Ball, J.M., et al., *Low-temperature processed meso-superstructured to thin-film perovskite solar cells.* Energy & Environmental Science, 2013. **6**(6): p. 1739-1743.
14. Burschka, J., et al., *Sequential deposition as a route to high-performance perovskite-sensitized solar cells.* Nature, 2013. **499**: p. 316.
15. Mitzi, D.B., *Organic−Inorganic Perovskites Containing Trivalent Metal Halide Layers: The Templating Influence of the Organic Cation Layer*. Inorganic Chemistry, 2000. **39**(26): p. 6107-6113.

16. O'Regan, B. and M. Grätzel, *A low-cost, high-efficiency solar cell based on dye-sensitized colloidal TiO2 films.* Nature, 1991. **353**(6346): p. 737-740.
17. Leijtens, T., et al., *Electronic Properties of Meso-Superstructured and Planar Organometal Halide Perovskite Films: Charge Trapping, Photodoping, and Carrier Mobility.* ACS Nano, 2014. **8**(7): p. 7147-7155.
18. Kim, H.-S., S.H. Im, and N.-G. Park, *Organolead Halide Perovskite: New Horizons in Solar Cell Research.* The Journal of Physical Chemistry C, 2014. **118**(11): p. 5615-5625.
19. Stranks, S.D., et al., *Electron-Hole Diffusion Lengths Exceeding 1 Micrometer in an Organometal Trihalide Perovskite Absorber.* Science, 2013. **342**(6156): p. 341-344.
20. Xing, G., et al., *Long-Range Balanced Electron- and Hole-Transport Lengths in Organic-Inorganic CH₃NH₃PbI₃*. Science, 2013. **342**(6156): p. 344-347.
21. Im, J.-H., et al. *Growth of CH3NH3PbI3 cuboids with controlled size for high-efficiency perovskite solar cells*. **9**, 927-932-927-932 DOI: 10.1038/Nnano.2014.181.
22. Giordano, F., et al., *Enhanced electronic properties in mesoporous TiO2 via lithium doping for high-efficiency perovskite solar cells.* Nature Communications, 2016. **7**: p. 10379.
23. Eperon, G.E., et al., *Morphological Control for High Performance, Solution-Processed Planar Heterojunction Perovskite Solar Cells.* Advanced Functional Materials, 2014. **24**(1): p. 151-157.
24. Jeng, J.-Y., et al., *CH3NH3PbI3 Perovskite/Fullerene Planar-Heterojunction Hybrid Solar Cells.* Advanced Materials, 2013. **25**(27): p. 3727-3732.
25. Docampo, P., et al., *Efficient organometal trihalide perovskite planar-heterojunction solar cells on flexible polymer substrates.* Nature Communications, 2013. **4**: p. 2761.
26. You, J., et al., *Low-Temperature Solution-Processed Perovskite Solar Cells with High Efficiency and Flexibility*. ACS Nano, 2014. **8**(2): p. 1674-1680.
27. Correa-Baena, J.-P., et al., *Promises and challenges of perovskite solar cells.* Science, 2017. **358**(6364): p. 739-744.
28. Jain, A., et al., *Performance of genetic algorithms in search for water splitting perovskites.* Journal of Materials Science, 2013. **48**(19): p. 6519-6534.
29. Kawamura, Y., H. Mashiyama, and K. Hasebe, *Structural Study on Cubic-Tetragonal Transition of CH3NH3PbI3*. Vol. 71. 2002. 1694-1697.

30. Chen, J., et al., *Recent progress in stabilizing hybrid perovskites for solar cell applications.* Journal of Power Sources, 2017. **355**: p. 98-133.
31. Stoumpos, C.C., C.D. Malliakas, and M.G. Kanatzidis, *Semiconducting Tin and Lead Iodide Perovskites with Organic Cations: Phase Transitions, High Mobilities, and Near-Infrared Photoluminescent Properties.* Inorganic Chemistry, 2013. **52**(15): p. 9019-9038.
32. M. Sanehira, E., et al., *The Influence of Electrode Interfaces on the Stability of Perovskite Solar Cells: Reduced Degradation using MoOx / Al for Hole Collection*. Vol. 1. 2016.
33. Niu, G., X. Guo, and L. Wang, *Review of recent progress in chemical stability of perovskite solar cells.* Journal of Materials Chemistry A, 2015. **3**(17): p. 8970-8980.
34. Cronin, H.M., et al., *Effects of ambient humidity on the optimum annealing time of mixed-halide Perovskite solar cells.* Nanotechnology, 2017. **28**(11): p. 114004.
35. Niu, G., et al., *Study on the stability of CH3NH3PbI3 films and the effect of post-modification by aluminum oxide in all-solid-state hybrid solar cells.* Journal of Materials Chemistry A, 2014. **2**(3): p. 705-710.
36. Park, N.-G., et al., *Towards Stable and Commercially Available Perovskite Solar Cells*. Vol. 1. 2016. 16152.
37. Snaith, H.J., et al., *Anomalous Hysteresis in Perovskite Solar Cells.* The Journal of Physical Chemistry Letters, 2014. **5**(9): p. 1511-1515.
38. Manser, J.S., J.A. Christians, and P.V. Kamat, *Intriguing Optoelectronic Properties of Metal Halide Perovskites.* Chemical Reviews, 2016. **116**(21): p. 12956-13008.
39. Noel, N.K., et al., *Lead-free organic–inorganic tin halide perovskites for photovoltaic applications.* Energy & Environmental Science, 2014. **7**(9): p. 3061-3068.
40. Zhu, H.L., et al., *Controllable Crystallization of CH3NH3Sn0.25Pb0.75I3 Perovskites for Hysteresis-Free Solar Cells with Efficiency Reaching 15.2%.* Advanced Functional Materials, 2017. **27**(11): p. 1605469.
41. Hoye, R.L.Z., et al., *Methylammonium Bismuth Iodide as a Lead-Free, Stable Hybrid Organic–Inorganic Solar Absorber.* Chemistry – A European Journal, 2016. **22**(8): p. 2605-2610.
42. Noh, J.H., et al., *Chemical Management for Colorful, Efficient, and Stable Inorganic–Organic Hybrid Nanostructured Solar Cells.* Nano Letters, 2013. **13**(4): p. 1764-1769.

43. Suárez Ramanzin, M.B., et al., *Recombination Study of Combined Halides (Cl, Br, I) Perovskite Solar Cells*. Vol. 5. 2014. 1628-1635.
44. Amat, A., et al., *Cation-Induced Band-Gap Tuning in Organohalide Perovskites: Interplay of Spin–Orbit Coupling and Octahedra Tilting.* Nano Letters, 2014. **14**(6): p. 3608-3616.
45. Chen, J., et al., *Mixed-Organic-Cation (FA)x(MA)1–xPbI3 Planar Perovskite Solar Cells with 16.48% Efficiency via a Low-Pressure Vapor-Assisted Solution Process.* ACS Applied Materials & Interfaces, 2017. **9**(3): p. 2449-2458.
46. Deng, Y., et al., *Air-Stable, Efficient Mixed-Cation Perovskite Solar Cells with Cu Electrode by Scalable Fabrication of Active Layer.* Advanced Energy Materials, 2016. **6**(11): p. 1600372.
47. Choi, H., et al., *Cesium-Doped Methylammonium lead Iodide Perovskite Light Absorber for Hybrid Solar Cells*. Vol. 7. 2014.
48. Niu, G., et al., *Enhancement of thermal stability for perovskite solar cells through cesium doping.* RSC Advances, 2017. **7**(28): p. 17473-17479.
49. Zheng, X., et al., *Improved Phase Stability of Formamidinium Lead Triiodide Perovskite by Strain Relaxation.* ACS Energy Letters, 2016. **1**(5): p. 1014-1020.
50. Nam, J.K., et al., *Potassium Incorporation for Enhanced Performance and Stability of Fully Inorganic Cesium Lead Halide Perovskite Solar Cells.* Nano Letters, 2017. **17**(3): p. 2028-2033.
51. Quan, L.N., et al., *Ligand-Stabilized Reduced-Dimensionality Perovskites.* Journal of the American Chemical Society, 2016. **138**(8): p. 2649-2655.
52. Smith, I.C., et al., *A Layered Hybrid Perovskite Solar-Cell Absorber with Enhanced Moisture Stability.* Angewandte Chemie International Edition, 2014. **53**(42): p. 11232-11235.
53. Yao, K., et al., *A general fabrication procedure for efficient and stable planar perovskite solar cells: Morphological and interfacial control by in-situ-generated layered perovskite.* Nano Energy, 2015. **18**: p. 165-175.
54. Cao, D.H., et al., *2D Homologous Perovskites as Light-Absorbing Materials for Solar Cell Applications.* Journal of the American Chemical Society, 2015. **137**(24): p. 7843-7850.

55. Safdari, M., et al., *Layered 2D alkyldiammonium lead iodide perovskites: synthesis, characterization, and use in solar cells.* Journal of Materials Chemistry A, 2016. **4**(40): p. 15638-15646.
56. Tsai, H., et al., *High-efficiency two-dimensional Ruddlesden–Popper perovskite solar cells.* Nature, 2016. **536**: p. 312.
57. Chen, Y., et al., *Tailoring Organic Cation of 2D Air-Stable Organometal Halide Perovskites for Highly Efficient Planar Solar Cells.* Advanced Energy Materials, 2017. **7**(18): p. 1700162.
58. Zhang, X., et al., *Stable high efficiency two-dimensional perovskite solar cells via cesium doping.* Energy & Environmental Science, 2017. **10**(10): p. 2095-2102.
59. Zhang, X., et al., *Vertically Oriented 2D Layered Perovskite Solar Cells with Enhanced Efficiency and Good Stability.* Small, 2017. **13**(33): p. 1700611.
60. Yao, K., et al., *Multilayered Perovskite Materials Based on Polymeric-Ammonium Cations for Stable Large-Area Solar Cell.* Chemistry of Materials, 2016. **28**(9): p. 3131-3138.
61. Gan, X., et al., *2D homologous organic-inorganic hybrids as light-absorbers for planer and nanorod-based perovskite solar cells.* Solar Energy Materials and Solar Cells, 2017. **162**: p. 93-102.
62. Grancini, G., et al., *One-Year stable perovskite solar cells by 2D/3D interface engineering.* Nature Communications, 2017. **8**: p. 15684.
63. Iagher, L. and L. Etgar, *Effect of Cs on the Stability and Photovoltaic Performance of 2D/3D Perovskite-Based Solar Cells.* ACS Energy Letters, 2018. **3**(2): p. 366-372.
64. Li, N., et al., *Mixed Cation FAxPEA1–xPbI3 with Enhanced Phase and Ambient Stability toward High-Performance Perovskite Solar Cells.* Advanced Energy Materials, 2017. **7**(1): p. 1601307.